Nascent-Chain Interaction Networks and Their Effect on the Bacterial Ribosome

Meranda M. Masse^a, Valeria Guzman-Luna^a, Angela E. Varela^{a,+}, Rachel B. Hutchinson^a, Aniruddha Srivastava^{a,‡}, Wanting Wei^{a°,} Andrew M.Fuchs^a and Silvia Cavagnero^a*

Department of Chemistry, University of Wisconsin-Madison, Madison, Wisconsin, 53706,
 USA.

Present Address

- ⁺A.E.V.: School of Veterinary Medicine, University of Wisconsin-Madison, Madison, Wisconsin, 53706, USA.
- [‡] A.S.: School of Medicine and Public Health, University of Wisconsin-Madison, Madison, Wisconsin, 53705, USA.
- ° W.W.: AIDS Vaccine Research Laboratory, University of Wisconsin-Madison, Madison, Wisconsin, 53711, USA.

Corresponding Author

* Email: cavagnero@chem.wisc.edu. Phone: 608-262-5430

Abstract

In order to become bioactive, proteins need to be biosynthesized and protected from aggregation during translation. The ribosome and molecular chaperones contribute to both tasks. While it is known that some ribosomal proteins (r-proteins) interact with ribosome-bound nascent chains (RNCs), specific interaction networks and their role within the ribosomal machinery remain poorly characterized and understood. Here, we find that RNCs of variable sequence and length (beyond the 1st C-terminal reside) do not modify the apparent stability of the peptidyl-transferase center (PTC) and r-proteins. Thus, RNC/r-protein interaction networks close to the PTC have no effect on the apparent stability of ribosome-RNC complexes. Further, fluorescence anisotropy decay, chemical-crosslinking and Western blots show that RNCs of the foldable protein apoHmp₁₋₁₄₀ have an N-terminal compact region (63–94 residues) and interact specifically with r-protein L23 but not with L24 or L29, at the ribosomal-tunnel exit. Longer RNCs bear a similar compact region and interact either with L23 alone or with L23 and another unidentified r-protein, or with molecular chaperones. The apparent strength of RNC/r-protein interactions does not depend on RNC sequence. Taken together, our findings show that RNCs encoding foldable protein sequences establish an expanding specific interaction network as they get longer, including L23, another r-protein and chaperones. Interestingly, the ribosome alone (i.e., in the absence of chaperones) provides indiscriminate support to RNCs bearing up to ca. 190 residues, regardless of nascent-chain sequence and foldability. In all, this study highlights the unbiased features of the ribosome as a powerful nascent-protein interactor.

Significance Statement

The presence of interactions between nascent chains bearing a foldable amino-acid sequence (with no signal or arrest tags) and specific ribosomal proteins has been suggested but never experimentally demonstrated, up to now. Here, we identify the ribosomal protein L23 as a specific nascent-chain-interacting partner. L23 establishes noncovalent contacts with nascent chains of the multi-domain foldable model protein apoHmp, which lacks signal/arrest sequences. Interactions with another ribosomal protein and with the trigger-factor and Hsp70 chaperones were also detected. Interestingly, ribosomal-protein/nascent-chain complexes have similar apparent stability regardless of nascent-chain sequence and degree of foldability. These findings are significant because they advance our knowledge on ribosome-mediated nascent-protein interaction networks and suggest avenues to prevent undesirable aggregation.

Introduction

Recent evidence suggests that the ribosome plays an active role in cotranslational protein folding (1-6). During translation, the nascent chain traverses the ribosomal exit tunnel, which is ca. 80-100 Å long, 10-35 Å wide (7-10) and can fit 30 to 40 nascent residues. (11-16) Within the ribosomal exit tunnel and its nearby regions across the highly negatively charged outer surface of the ribosome, (3) nascent chains encoding single-domain proteins become compact (17, 18) and acquire some secondary (19-23) and tertiary structure (5, 24-28). This set of observations proves the importance of the ribosome in nascent-protein structure formation.

During translation, the ribosome influences nascent protein chains at different levels. For instance, the inner geometry of the ribosomal exit tunnel favors formation of secondary nascent-chain structure, especially of α -helical (22, 29-31) or β -sheet nature (23). In addition, recent work showed that the ribosomal exit tunnel and vestibule enable acceleration of folding – but not unfolding – of a small single-domain protein, thereby stabilizing nascent protein chains relative to their free state in solution (32). On the other hand, the ribosome may also destabilize single-protein domains, in case the domain is far removed from the peptidyl transferase center (33). Further, the ribosome renders nascent chains soluble relative to the corresponding ribosome-released protein chains, thereby supporting cotranslational folding (34). Collectively, these results highlight the influence of the ribosome on nascent protein folding.

The ribosome is known to establish physical noncovalent interactions with nascent chains. As summarized in Table 1, these interactions have been identified in a variety of experimental studies and can be divided into three categories. Namely, (i) interactions between the ribosome and nascent chains carrying an N-terminal signal sequence (22, 35-39), (ii) interactions between the ribosome and nascent chains bearing C-terminal ribosome-stalling or arrest sequences (40-47),

and (iii) interactions between nascent chains that lack N- or C-terminal ribosome-stalling or arrest sequences (48). Additional studies are consistent with the presence of ribosome-nascent-chain interactions, though they do not directly prove their existence (49-52).

While a body of research has explicitly addressed how the ribosome influences nascent polypeptides and proteins, little is known about how the nascent chain affects the properties of the ribosome. For instance, empty 70S ribosomes are known to be more prone to dissociation than ribosomes bearing both mRNA and peptidyl tRNA. This conclusion was reached upon addition of either ribosome-dissociation factors (53) or Hofmeister cosolutes (54-56). Other researchers established a similar finding upon depletion of magnesium ions (57-59). In a different study, addition of Hofmeister salts were employed to show that translation initiation complexes (including 70S in complex with initiator tRNA) disassemble more easily than peptidyl tRNAs bearing nascent chains (60). In this work, ribosomes carrying longer nascent chains were found to be less prone to dissociation (60). Other work has examined the effect of magnesium ions and other Hofmeister ions on empty 70S ribosome disassembly and how it changes sedimentation coefficients (61).

Yet, there is only a limited number of studies targeting the effect of non-Hofmeister denaturing agents on the ribosome. For instance, it is known that the 30S subunit disassembles in the presence of 6 molar urea (62). In addition, urea lowers the melting temperature and sedimentation coefficient of the 50S ribosomal subunit (63). The 30S subunit is more sensitive to thermal denaturation than the 50S subunit, and the 70S ribosome is most thermally stable (64). Most notably, 70S ribosomes bearing a nascent chain are less prone to chemical denaturation than empty ribosomes (33).

However, the effect of urea on the disassembly of various ribosome components (e.g. peptidyl transferase center -- a.k.a. PTC -- and ribosomal proteins) as a function of specific RNC characteristics (e.g., length and amino-acid sequence, interactions with ribosomal proteins) has not been characterized yet, to date. The present work moves initial steps towards filling this gap of knowledge.

We find that short peptidyl-tRNAs (snc-tRNAs) stabilize the 70S ribosome against denaturation by the non-Hofmeister cosolute urea, and we propose a multi-step model for the disassembly of ribosome-RNC complexes consistent with our findings. In addition, RNCs up to chain length 140 interact only with one ribosomal protein (r-protein), i.e., L23, in the vicinity of the tunnel exit. A wider interaction network, including one additional ribosomal protein and the trigger factor (TF) and Hsp70 chaperones, gets established as the nascent chain elongates further. Finally, our data also suggest that the interaction strength of individual RNC/r-protein populations does not vary significantly with RNC sequence and length. In all, our results show that (a) the interaction of foldable RNCs with the L23 ribosomal protein has been explicitly identified experimentally for the first time, and (b) the ribosome provides even, indiscriminate assistance to newly synthesized nascent protein chains, whether they are foldable or intrinsically disordered, via a powerful and highly specific interaction network.

Results and Discussion

The presence of very short nascent chains stabilizes the 70S ribosomal complex. We started our investigations by performing a series of sucrose-gradient studies on *E. coli* empty ribosomes and nascent-chain-loaded ribosomes. Our results, detailed in SI-Appendix Figure S1 and S3, showed that empty-70S ribosomes are more sensitive to urea denaturation than ribosomes bearing

tRNAs linked to longer nascent chains. It appears that the aminoacyl-tRNA is responsible for most of the stabilizing effect (SI-Appendix, Figs. S1 and S3). Interestingly, the length and amino-acid sequence of the nascent protein does not influence the urea sensitivity of ribosome-RNC complexes.

The sequence dependence of ribosome-nascent-chain interactions has been further explored in other parts of this work.

Extending the nascent-protein-chain portfolio. The experiments described in the next sections employed a larger set of RNCs than the sucrose-gradient studies. Our specific purpose was to test the effect of RNC chain length, sequence and foldability on the apparent stability of the ribosome and to experimentally characterize the RNC-ribosome interaction network. First, we examined several constructs derived from the *Escherichia coli* protein flavohemoglobin (apoHmp). The structure and key building blocks of this protein analyzed in this work shown in Figure 1a,b. The crystal structure of apoHmp comprises three domains, an N-terminal heme-binding (domain 1), a flavin adenine dinucleotide-binding (domain 2) and a C-terminal nicotinamide adenine dinucleotide-binding domain (domain 3), as schematically illustrated in Figure 1b (65). Hmp plays a key role in O₂, NO and CO transport in *E. coli* and is involved in a variety of signaling pathways (66, 67). We also studied the behavior of the phosphorylated insulin receptor interacting region of the growth factor receptor-bound protein 14 (Grb14) from *Rattus norvegicus*. This protein, which is denoted here as PIR, is intrinsically disordered (68), i.e., an IDP. The specific nascent chain constructs of both proteins analyzed in this work are illustrated in SI-Appendix Figure S4.

Ribosome-bound apoHmp nascent chains of variable length are compact. Next, we performed fluorescence depolarization decay experiments in the frequency domain (69-71) to probe the rotational dynamics of nascent chains encoding foldable sequences. This technique has been

previously employed to assess the rotational correlation time (τ_c) and amplitude of rotational motions of RNCs (17, 18, 34, 49, 72). The goal of this experiment was to probe whether RNCs harboring long nascent chains display any degree of compaction. We focused on RNCs of apoHmp₁₋₁₄₀, corresponding to the N-terminal domain 1 of Hmp, and RNCs of apoHmp₁₋₁₈₉, comprising Hmp domain 1 plus 49 C-terminal residues belonging to domain 2. Nascent proteins were site-specifically labeled at their N terminus with the BODIPY-FL fluorophore as described (17). Once information on nascent-chain compaction is in hand, the interplay between ribosome and nascent-chain sensitivity to urea denaturation can be more rationally explored and understood, as apparent in the sections below.

Representative data for apoHmp₁₋₁₄₀ and apoHmp₁₋₁₈₉ are shown in panels c and d of Figure 1, respectively. Both RNCs display informative frequency-domain anisotropy decay profiles. As shown in Figure 1e and consistent with the very low reduced χ^2 values, the fits that include 3 rotational-tumbling components give the best results. Importantly, panels e and f of Figure 1 show that both apoHmp₁₋₁₄₀ and apoHmp₁₋₁₈₉ RNCs are characterized by an N-terminal compact domain. In both cases, this domain spans ca. 63 to 94 residues, depending on the exact shape. Note that RNC shape assessment is beyond the scope of this work. Regardless of the actual overall morphology of the compact domains, the fact that a similar-size compact domain is observed for both apoHmp₁₋₁₄₀ and apoHmp₁₋₁₈₉ suggests that both constructs undergo some partial folding on the ribosome. Surprisingly, the observed size of the compact domain of apoHmp₁₋₁₈₉ RNCs is significantly smaller than domain 2, which comprises 140 residues (Fig. 1b). Therefore, biosynthesis of the additional 49 C-terminal amino acids is not sufficient to lead to complete folding of the N-terminal domain, for this protein.

In addition, the cone semi-angle analysis of the fluorescence anisotropy decay data (Fig. 1f) shows that the compact domain of Hmp_{1-189} RNCs spans a slightly wider cone semi-angle $(26.5^{\circ} \pm 0.5^{\circ} \ vs \ 20^{\circ} \pm 0.2^{\circ})$ than Hmp_{1-140} RNCs, consistent with the fact that the latter construct is likely projecting further out from the ribosomal surface than the shorter Hmp_{1-140} construct.

In all, the fluorescence anisotropy data show that the Hmp₁₋₁₄₀ and Hmp₁₋₁₈₉ nascent chains are both comparably compact and no more than partially folded, while on the ribosome, with Hmp₁₋₁₈₉ spanning a slightly wider cone semi-angle.

The peptidyl transferase center site is largely unaffected by nascent-chain sequence and length, beyond 32 residues. Next, we probed whether nascent chains of different length, amino-acid sequence and foldability affect the apparent stability of specific regions of the ribosome. We directed our focus on the peptidyl transferase center (PTC) of the *E. coli* ribosome, and we explored its urea sensitivity via a nascent-chain ribosome-release assay mediated by puromycin. The results of puromycin-release-detected urea titrations are shown in the SI Appendix Figure S5 and further described in the SI Appendix. Overall, the urea titration data show that the nature of the nascent chain has a weak effect on the urea sensitivity of the PTC, in *E. coli*. Next, we explored the effect of nascent-chain properties on the apparent stability of ribosomal proteins.

The global urea sensitivity of ribosomal proteins is largely unaffected by nascent-chain sequence and length. The global urea sensitivity of ribosomal proteins (r-proteins) was probed via urea titrations based on Trp fluorescence emission. Trp is a well-known fluorescent reporter, and its emission properties are highly environmentally sensitive. Upon inspection of the *E. coli* ribosomal-protein sequences via the 2WWL and 2WWQ Protein Data Bank (PDB) files, we ascertained that the r-proteins of the ribosome comprise a total of 32 Trps (SI-Appendix Fig. S6a) roughly uniformly dispersed throughout the ribosomal structure. To gain insights at the highest

possible resolution, we focused on all the apoHmp nascent chains listed in SI-Appendix Figure S4e, and on the PIR nascent chain, also listed in the same figure. Note that apoHmp nascent chains only contribute two additional Trps at positions 120 and 149, and PIR only contributes on Trp at position 44. We regard these residues, present in some of the constructs, as contributing negligibly to the overall Trp fluorescence emission. In essence, the readout of this assay is dominated by the much larger contributions arising from the 32 Trps interspersed across the r-proteins. Urea titrations were carried out and Trp fluorescence emission was monitored (SI-Appendix Fig.S6b). Spectral shifts were regarded as reporters of r-protein folding, and centers of mass of emission spectra were assessed to generate titration curves reporting on the urea sensitivity of r-proteins. Urea titration data were processed according to Santoro and Bolen (73, 74). Individual representative titration curves are shown in SI-Appendix Figure S6d.

The $\Delta G^{\circ}_{app, unfold}$ for each construct are plotted in SI-Appendix Figure S6e and corresponding t-test values are tabulated in SI-Appendix Figure S6f. Nearly all the constructs show statistically similar results, with $\Delta G^{\circ}_{app, unfold}$ values ranging from 2 to 5 kcal/mol. Hence, the presence of peptidyl tRNA, regardless of nascent-chain characteristics, does not affect the urea sensitivity of r-proteins. As shown in sections below, some nascent chains interact with specific ribosomal proteins. On the other hand, these interactions are not sufficiently strong to be detected via this assay, which monitors the overall sensitivity to urea of all r-proteins.

Nascent chains of apoHmp₁₋₁₄₀ and apoHmp₁₋₁₈₉ interact with ribosomal protein L23. The data of SI-Appendix Figure S6 showed that the apparent stability of r-proteins is not influenced by the presence of either intrinsically disordered or foldable nascent chains of variable length and physical properties. On the other hand, nascent chains encoding the intrinsically disordered protein PIR are known to interact with the r-protein L23 and L29 (48). It is reasonable to imagine that

these interactions are not sufficiently strong to be detected by the Trp-fluorescence assay of SI-Appendix Figure S6, which monitors Trp environment across the entire ribosome. Hence, the data in SI-Appendix Figure S6 do not preclude the presence of RNC/ribosome interactions. Hence, it is compelling to explore whether these interaction exist. As shown in Figure 2a, the *E. coli* ribosome comprises several proteins within the region near the exit-tunnel.

In this work, we focused on the L23, L24 and L29 r-proteins, which are closest to the vestibule and outer region of the ribosomal exit tunnel. We explored the interaction patterns of the apoHmp₁-₁₄₀ and apoHmp₁₋₁₈₉ nascent chains, which populate compact states while ribosome-bound (Fig. 1 c-g). The well-characterized zero-length chemical crosslinker carbodiimide 1-ethyl-3-[3dimethylaminopropyl] carbodiimide hydrochloride (EDC) was employed (48, 75, 76). To carry out chemical crosslinking of nascent chains, we followed known procedures (48) involving a combination of low-pH SDS-PAGE (77) and Western blotting in the absence and presence of the trigger factor (TF) chaperone. Notably, EDC enables detecting existing noncovalent interactions, though it does not provide an accurate quantitation of interacting populations, as discussed at length by Guzman-Luna et al. (48). Yet, EDC is an extremely valuable tool to detect proteinprotein interactions within the ribosome-nascent-chain complex. Site-specific fluorescence labeling of nascent proteins at their N terminus enables focusing exclusively on interactions involving the nascent protein. Low-pH-gel and Western-blot were collected to explore interactions between nascent chains and r-proteins. These interactions have not been directly detected before, in the case nascent chains lacking arrest or signal sequences. It is worth noting that EDC does not have high accessibility within the exit-tunnel core (48). Therefore, detecting interactions within the tunnel core, including corresponding Western-blotting work, would not have been informative within our experimental setup.

It is also important to mention that, under our experimental conditions, EDC does not report on interactions involving nascent protein chains and ribosomal RNA (rRNA). In the presence of imidazole, crosslinks between RNA 5' phosphate and aliphatic amines of proteins is known to take place (75). However, our samples did not contain imidazole, and this chemical would anyways be unable to detect interactions not involving the 5' end of RNA. Therefore, even in the presence of imidazole, EDC would likely underestimate all potential interactions with RNA. Thus, interactions between nascent proteins and r-RNA are beyond the scope of this study.

The data for apoHmp₁₋₁₄₀ and apoHmp₁₋₁₈₉, shown in Figures 2c and 3a,b, respectively, indicate that both nascent proteins interact with ribosomal protein L23. Western blotting was also carried out with antibodies against ribosomal proteins L24, L29 (SI Appendix, Figs. 9 and 11). However, no interactions between these two r-proteins and apoHmp₁₋₁₄₀ and apoHmp₁₋₁₈₉ were detected.

These results show for the first time that two RNCs lacking signal or arrest sequences and encoding nascent proteins that partially fold on the ribosome experience interaction with a specific ribosomal protein. The intrinsically disordered PIR RNC, which was studied before (48), was found to have a ca. 50% population of RNC interacting with L23 and L29. In contrast, here we use two nascent chains corresponding to the foldable apoHmpHa₁₋₁₄₀ and apoHmp₁₋₁₈₉ sequences, whose N-terminal regions are compact (Fig. 1 c-g). These apoHmpH RNCs interact only with L23 and not with L29.

The interactions experienced by apoHmp₁₋₁₄₀ and apoHmp₁₋₁₈₉ involve the dominant fraction of the apoHmpH RNC population, which is found to nearly-quantitatively crosslink with the L23 ribosomal protein (Fig. 2 and 3). This scenario is different from the case of intrinsically disordered PIR RNCs, (48) which crosslink only in part, under the same experimental conditions. The larger extent of crosslinking of the foldable apoHmp₁₋₁₄₀ and apoHmp₁₋₁₈₉ nascent chains, however, may

simply result from the greater number of EDC-reactive residues of apoHmp₁₋₁₄₀ (25 EDC-reactive residues, 20 beyond the tunnel core) and apoHmp₁₋₁₈₉ (36 EDC-reactive residues, 30 beyond the tunnel core) relative to PIR (14 EDC-reactive residues, 12 beyond the tunnel core). Interestingly, as shown in the sections below, the urea sensitivity of the L23-RNC complexes is similar for all RNCs, suggesting comparable interaction strengths.

Importantly, given that the fluorescence anisotropy-decay data of Figure 1 show that RNCs of both apoHmp₁₋₁₄₀ and apoHmp₁₋₁₈₉ have "freely tumbling" compact regions, our data suggest that the compact regions are not engaged in direct interactions with the ribosomal surface.

In the case of apoHmp₁₋₁₈₉, there is an additional interacting population, which we denoted as RP2 (Fig. 5). This population includes r-protein L23 (Fig. 3b) and one additional unidentified protein of c.a. 6-10 kDa. Our Western Blots indicate that L29 (7 kDa) is not present in the RP2 band (SI Appendix, Fig. S11b), based on molecular-weight arguments. Other cytoplasmic *E. coli* chaperones and ribosome interactors (GroEL, GroES, SecB, K/J/E, SRP and ClpB; MW range: 48-80 kDa) are ruled out as they would appear well above the RP2-containing band in our gels (Fig. 3). Because of its close spatial proximity to L23 (Fig. 2a) and based on molecular weight arguments, we believe that it is possible that RP2 comprises L23 and L29. However, our monoclonal antibodies were not able to capture an L29 epitope, suggesting the utility of experiments employing polyclonal L29 antibodies. These are experiments are planned in future investigations.

Finally, the data for Figures 4 and 5 also show that a fraction of the RNCs interacts with the trigger factor (TF) chaperone (presumably coupled to the ribosome via L23), rather than with the L23 r-protein. The role of the interactions between apoHmpH RNCs and TF are beyond the scope of this work and have already been explored elsewhere in the case of other client proteins. (39, 78-

81) These studies showed that TF interacts with clients that bear an expanded conformation in their bound state.

In all, our data show that apoHmpH₁₋₁₄₀ and apoHmp₁₋₁₈₉ RNCs interact with either the L23 r-protein or with the TF chaperone. We propose that these two classes of interactions may play a similar role, and that therefore L23 may be a chaperone-like ribosomal protein that contributes to maintaining RNC solubility during translation. Future studies will focus on genetic r-protein modifications aimed at disrupting the detected interactions. The large surface-exposed nonpolar patch of the L23 ribosomal protein (Fig. 2b) suggests that the interactions involving apoHmp₁₋₁₄₀ and apoHmp₁₋₁₈₉ RNCs may be contributed by the hydrophobic effect. This nonpolar patch appears an ideal candidate for genetic modifications aimed at significantly perturbing RNC/r-protein interactions.

Nascent chain-L23 complexes have the same apparent stability regardless of RNC sequence.

To further explore the nature of the interactions between the L23 r-protein and nascent chains of increasing length and variable sequence, we performed urea titrations with chemical crosslinking detection (Fig. 4a,b). EDC readily reacts with amines and carboxylic acid functional groups, and there is no loss of EDC reactivity even in the presence of high urea concentrations (82). It is worth noting that the interactions identified in this work are not induced by the covalently N-terminal-linked BODIPY-502 fluorophore, as previous work has shown that this fluorophore does not interact with resuspended ribosomes under conditions like those of the present study (17). Therefore, by unfolding the complex in the presence of urea and subsequently adding EDC, we expect to gain insights into the urea sensitivity of nascent chain-L23 complexes. After collecting gel data on representative apoHmp and PIR nascent chains (Fig. 4c), we estimated the apparent stability (ΔG°_{app,unfold}) of nascent chain-L23 complexes following procedures similar to the other

urea titrations described earlier (73). Representative EDC-mediated urea titrations are shown in Figure 6c. Corresponding plots and apparent-stability data are displayed in Figure 4e,f. The matching two-tailed Student's t-test is provided in Figure 6g. As shown in Figure 4h, the apparent stability values for the apoHmp and PIR nascent-chain/L23 complexes range between ca. 2 and 5.5 kcal/ mol. Remarkably, all complexes display the same urea sensitivity within error. This is true even though the nascent-chain portions that are not buried within the exit-tunnel core have widely different nonpolar and net-charge-per-residue content (Fig. 4i) and widely different total nonpolar surface accessible surface-area values (Fig. 4j).

In summary, the urea-titrations in Figure 4 show that the urea sensitivity of r-proteinnascent-chain complexes is similar regardless of the nature and length of the nascent chain, across the short and long (55- to 189-residue) chains examined here. In other words, RNC/-r-protein complexes have the same apparent stability although the RNCs have widely different physical properties and compaction, as discussed above and, in the case of PIR lack of compaction, in previous work. (48, 49) A cartoon showing a low-resolution RNC model consistent with the crosslinking and fluorescence-anisotropy data is shown in Figure 1c-g. Further, the longer RNCs of apoHmp₁₋₁₈₉ also exhibit interactions with an additional yet-unidentified r-protein. The corresponding crosslinked complex is denoted as RP2 in Figure 3 and Figure 5. At this juncture, a few additional considerations come to mind. First, the 55- and 140-residue nascent chains of apoHmp lack or include the N-terminal 65-94-residue compact region detected via fluorescence anisotropy decay (Fig. 1c-g), respectively. Therefore, the non-compact C-terminal portion of the nascent chain out of the tunnel core seems to be primarily engaged in the detected interactions with the L23 r-protein in the case of apoHmp. Given that the amino-acid sequences of the interacting regions of apoHmp₁₋₅₅ and apoHmp₁₋₁₄₀ must be different yet the interactions are of comparable apparent strength, the interactions seem to be of nonspecific nature, amounting to an overall sufficient affinity the 100% interacting population detected in the gels of Figure 5. Second, apoHmp₁₋₁₄₀ and apoHmp₁₋₁₈₉ are also found to experience interaction of equivalent apparent strength with L23 (see RP1 gel bands in Fig. 4d and g). On the other hand, apoHmp₁₋₁₈₉ also experiences interactions with another r-protein (see RP2 band in Fig. 4d). This finding supports the idea that the RNC-r-protein contacts are of somewhat non-specific nature and longer RNCs interact with additional ribosomal surface, likely engaging a longer portion of their chain. Finally, previous work showed that the interactions experienced by PIR₁₋₉₁ are ca. 50% mediated by Mg⁺² ions (48). Yet the apparent strength of these interactions is not different from that experienced by the other nascent chains, suggesting that all interactions are relative weak and non-specific (Fig. 4 f-h). This model is consistent with the fact RNC-r-protein interactions likely need to be continuously remodeled, as nascent chains elongate during translation. In all, the nature (Mg⁺² dependence, nonpolar *vs* electrostatic, or else) of RNC-r-protein interactions is still poorly understood and clearly awaits future higher-resolution structural investigations.

Nascent chain and r-protein interaction strength does not vary in the presence of one or more molecular chaperone. Next, we explored the effect of molecular chaperones TF and Hsp70 on the RNC-r-protein interactions via the same type of EDC-mediated urea titrations employed in the last two sections. The Hsp70 chaperone was examined holistically as the as Dnak/DnaJ/GrpE chaperone system, denoted here as K/J/E. TF is known to associate with prokaryotic ribosomes (83) and K/J/E works in cooperation with TF (84) to promote nascent-protein folding and prevent their aggregation (85-88).

First, we evaluated apoHmp₁₋₁₈₉ devoid of both TF and the Hsp70 chaperone system (K/J/E), apoHmp₁₋₁₈₉ in the presence of low concentrations of TF only, apoHmp₁₋₁₈₉ in the

presence of low concentrations of K/J/E only, and apoHmp₁₋₁₈₉ in the presence of both chaperones at low concentration (Fig. 5a). Urea titrations were carried out using increasing concentrations of urea (Fig. 5b), and the intensity of the crosslinked fraction was plotted as a function of urea (Fig. 5c). We then obtained a ΔG°_{app, unfold} values for each of these constructs (Fig. 5d) and evaluated them with a two-tailed Student's t-test (Fig. 5g). Interestingly, in all construct variations tested, the apparent strength of the L23-nascent chain complex was found to be statistically similar (Fig. 5f, h). Because this effect is not due to an increase or decrease in the fraction of crosslinked nascent chains to r-proteins (Fig. 5e, f). Via Western Blot analysis, we were able to conclude that interactions mainly take place with r-protein L23 (Fig. 3, b and SI Appendix, Fig. S11). This finding is consistent with our assessment of interacting proteins from apoHmp₁₋₁₄₀ (Fig. 2 and SI Appendix, Fig. S9). This result suggests that in both the presence and absence of one or more molecular chaperones, nascent chains interact with ribosomal L23 in a structurally similar manner, though future work will need to be employed to validate this claim.

To further elucidate the nature of nascent chain and molecular chaperones, we performed experiments using increasing concentrations of TF and K/J/E in the presence of EDC (Fig. 5i, j). Briefly, interactions with r-protein L23 can be displaced by high concentrations of molecular chaperones (8 μM TF and 10/2/4 μM K/J/E, respectively, Fig. 5c,d). A low pH SDS-PAGE gel reporting on apoHmp₁₋₁₈₉ RNCs shows that at low concentrations of TF and K/J/E (2-15 nM of TF and 0.5 μM, 0.04μM and 0.05μM of and DnaK, DnaJ and GrpE respectively), interactions with two r-proteins are established (Fig. 5i, gel lanes 1 and 2). Corresponding lanes in the Western Blot of this gel against L23 show that interactions involve r-protein L23 (Fig. 5i, Western Blot lanes 1 and 2). Interestingly, at high TF concentration (8 μM) Fig. 5i, gel lane 3), all r-protein interactions are displaced and replaced by contacts with TF (Fig. 5i, Western Blot lane 3). TF and L23 are

known to interact with one another on the ribosome (78, 80, 88), though we presently cannot explicitly discriminate whether the nascent chains interacts with L23 and TF, or if the nascent chain interacts with TF, which in turn interacts with L23. Here, we propose the simplest scenario namely that RNCs interact with TF only and, in turn, TF interacts with L23, which is known to be the TF docking site on the ribosome (2).

Similarly, interactions with r-proteins are also displaced by increased concentrations of K/J/E (10/2/4 μM K/J/E, respectively), although no interactions with L23 were detected when K/J/E concentrations are increased (Fig. 5i Western Blot lane 4), L24 or L29 (SI Appendix, Fig. S11), suggesting that the nascent chain likely does not interact with any r-proteins (Fig. 5i Western Blot lane 4). Similar results are seen for apoHmp₁₋₁₄₀ (SI Appendix, Fig. S9). Figure 5b and c shows model of the interaction interplay between nascent chains (c.a. length of 140-190 amino acids), r-proteins and molecular chaperones assessed in this work.

To summarize, when TF and K/J/E are not present, the nascent chain interacts with r-proteins only. In experiments with low concentrations of molecular chaperones (2-15 nM of TF and 0.5 μM, 0.04μM and 0.05μM of and DnaK, DnaJ and GrpE respectively, Fig. 7i,j), RNCs interact with TF but not K/J/E. At high, physiologically relevant concentrations of TF and K/J/E (8 μΜ TF and 10/2/4 μΜ K/J/E, respectively), RNC interactions with r-proteins are displaced by interactions with molecular chaperones. It is worth nothing that TF and K/J/E chaperones are shared with thousands of additional cellular proteins *in vivo*, unlike in the experiments shown here, which include purified resuspended RNCs. Further, our RNC concentrations are only 20-30 nM. Hence, chaperones are in large excess over RNCs even at the low chaperone concentrations employed here. This scenario differs from the cellular environment where both RNCs and molecular chaperones are at comparable concentrations, within the low uM range. Therefore, we

propose that the actual cellular milieu likely involves RNC populations that interact in part with TF and K/J/E and in part with r-proteins.

Concluding remarks on the RNC interaction network experienced by the foldable apoHmpH protein. An overall model recapitulating the main features of the RNC interactions network elucidated in this work in shown in Figure 6. Briefly, RNCs encompassing the entire N terminal domain of apoHmpH (apoHmp₁₋₁₄₀) experience either interactions with the L23 r-protein accompanied by independent tumbling of the N-terminal region or interactions with the TF chaperone (Fig. 6a). On the other hand, RNCs comprising the entire N terminal domain of apoHmpH and additional 49 residues belonging to the second domain (apoHmp₁₋₁₈₉) are subject to either similar interactions with the L23 r-protein, or to interactions with L23 and one additional presently unidentified protein (RP2), or to interactions with TF (Fig. 6b). Finally, in the presence of an excess of either TF or the Hsp70 chaperone system at total concentrations matching cellular levels, the interactions with ribosomal proteins are replaced by interactions with the respective molecular chaperones (Fig. 6c-d). The emerging scenario resulting from our work suggests that the ribosome plays an RNC-interacting role entirely like that of molecular chaperones.

In all, our findings highlight the prominent role of the ribosome as an RNC interactor and suggest that the ribosome may have played a primordial chaperone role in Nature, before the evolution of molecular chaperones.

Materials and Methods

Preparation of empty ribosomes. Empty ribosomes were generated from an in-house-prepared A19 WT or A19 Δ tig *E. coli* S30 cell extract as described (17, 89). Briefly, cells were grown in Luria-Bertani (LB) broth and harvested at mid-log phase ($A_{600} \sim 0.6$). The cells were lysed through

a French press (thermo Electron Corporation, Waltham, MA) at ~12,000 psi with a single passage. The lysate was subject to centrifugation at 30910 g and 20 °C for 20 min. After centrifugation, the supernatant was incubated in translation buffer (0.75 M Tris-HCl pH 8.2, 7.5 mM DTT, 21 mM Mg(OAc)₂, 500 μM amino acids, 6 mM ATP, 67 mM PEP and 160 μg/mL pyruvate kinase) for 80 min to remove any endogenous mRNA from ribosomes. The supernatant was then dialyzed (12-14 kDa MWCO) in buffer (10 mM Tris-HCl pH 8.2, 14 mM Mg(OAc)₂, 60 mM KOAc and 1 mM DTT) for 12 hrs, with a buffer exchange every 4 hours. The resulting A19 cell extract was used as the empty-ribosome sample.

Preparation of RNCs. RNCs were generated using an in-house prepared A19 *E. coli* transcription-translation coupled cell-free system (17, 89) as described. Cell strains either including (WT) or lacking (Δtig) the trigger factor gene were employed (17, 89). Hsp70 chaperone activity was suppressed via the KLR-70 peptide (90) to a final concentration of 0.2 mM. Transcription-translation proceeded for 30 min at 37 °C in the presence of BODIPY-FL-Met-tRNA^{E-Met} to specifically label RNCs at the N terminus. BODIPY-FL-Met-tRNA^{E-Met} was prepared as described (17). RNCs were stalled at various lengths to generate the desired apoHmp and PIR constructs via oligodeoxynucleotide-directed mRNA cleavage (17, 91, 92). An anti-ssrA oligonucleotide (17) was added to a final concentration of 12.83 pmol/μL to prevent premature release of stalled RNCs. RNC pellets were isolated via a sucrose cushion (1.1 M sucrose, 20 mM tris base, 10 mM Mg(OAc)₂, 500 mM NH₄Cl, and 0.5 mM EDTA, 1 mM DTT, pH 7.0, as described)(17) and subjected to ultracentrifugation at 160,000 g for 1 hr at 4 °C. The purified pellet was dissolved in resuspension buffer (10 mM tris-HCl, 10 mM Mg(OAc)₂, 60 mM NH₄Cl, 0,5 mM EDTA and 1.0 mM DTT, pH 7.0) by shaking in an orbital shaker at 200 rpm on ice for 1 hr.

Other experimental procedures. Details on sucrose gradients, low-pH gels, puromycin assays, chemical crosslinking and urea titrations are available in the SI Appendix.

Acknowledgments

We are thankful to M. Dalphin for helpful discussions. This work was funded by the National Science Foundation (NSF) grants MCB-1616459 and MCB-0951209 (to S.C). M. M. M. and R.B.H. received NIH TEAM-Science Fellowships from the University of Wisconsin-Madison and M.M.M received the Straka Fellowship from the University of Wisconsin-Madison. A. E. V. received a National Science Foundation GRFP graduate fellowship and a Science and Medicine Graduate Research Scholars Fellowship from the University of Wisconsin-Madison.

REFERENCES

- D. N. Wilson, R. Beckmann, The ribosomal tunnel as a functional environment for nascent polypeptide folding and translational stalling. *Curr. Opin. Struct. Biol.* 21, 274-282 (2011).
- 2. G. Kramer, D. Boehringer, N. Ban, B. Bukau, The ribosome as a platform for cotranslational processing, folding and targeting of newly synthesized proteins. *Nat. Struct. Mol. Biol.* **16**, 589 (2009).
- 3. D. V. Fedyukina, S. Cavagnero, "Protein Folding at the Exit Tunnel" in Annual Review of Biophysics, D. C. Rees, K. A. Dill, J. R. Williamson, Eds. (Annual Reviews, Palo Alto, 2011), vol. 40, pp. 337-359.
- 4. S. Pechmann, F. Willmund, J. Frydman, The ribosome as a hub for protein quality control. *Mol. Cell* **49**, 411-421 (2013).
- 5. M. Liutkute, E. Samatova, M. V. Rodnina, Cotranslational folding of proteins on the ribosome. *Biomolecules* **10**, 97 (2020).
- 6. C. A. Waudby, C. M. Dobson, J. Christodoulou, Nature and Regulation of Protein Folding on the Ribosome. *Trends Biochem. Sci.* **44**, 914-926 (2019).
- 7. N. Ban, P. Nissen, J. Hansen, P. B. Moore, T. A. Steitz, The complete atomic structure of the large ribosomal subunit at 2.4 Å resolution. *Science* **289**, 905-920 (2000).
- 8. J. Harms *et al.*, High resolution structure of the large ribosomal subunit from a mesophilic eubacterium. *Cell* **107**, 679-688 (2001).
- 9. P. Nissen, J. Hansen, N. Ban, P. B. Moore, T. A. Steitz, The Structural Basis of Ribosome Activity in Peptide Bond Synthesis. *Science* **289**, 920-930 (2000).

- 10. N. Voss, M. Gerstein, T. Steitz, P. Moore, The geometry of the ribosomal polypeptide exit tunnel. *J. Mol. Biol.* **360**, 893-906 (2006).
- 11. L. I. Malkin, A. Rich, Partial resistance of nascent polypeptide chains to proteolytic digestion due to ribosomal shielding. *J. Mol. Biol.* **26**, 329-346 (1967).
- 12. G. Blobel, D. Sabatini, Controlled proteolysis of nascent polypeptides in rat liver cell fractions: I. Location of the polypeptides within ribosomes. *The Journal of cell biology* **45**, 130-145 (1970).
- 13. S. Wang, H. Sakai, M. Wiedmann, NAC covers ribosome-associated nascent chains thereby forming a protective environment for regions of nascent chains just emerging from the peptidyl transferase center. *The Journal of cell biology* **130**, 519-528 (1995).
- 14. G. Kramer, V. Ramachandiran, B. Hardesty, Cotranslational folding—omnia mea mecum porto? *The international journal of biochemistry & cell biology* **33**, 541-553 (2001).
- 15. T. Tsalkova, O. Odom, G. Kramer, B. Hardesty, Different conformations of nascent peptides on ribosomes. *J. Mol. Biol.* **278**, 713-723 (1998).
- 16. C. A. Woolhead, P. J. McCormick, A. E. Johnson, Nascent Membrane and Secretory Proteins Differ in FRET-Detected Folding Far inside the Ribosome and in Their Exposure to Ribosomal Proteins. *Cell* 116, 725-736 (2004).
- 17. J. P. Ellis, C. K. Bakke, R. N. Kirchdoerfer, L. M. Jungbauer, S. Cavagnero, Chain dynamics of nascent polypeptides emerging from the ribosome. *Acs Chemical Biology* 3, 555-566 (2008).
- 18. R. B. Hutchinson, X. Chen, N. Zhou, S. Cavagnero, Fluorescence Anisotropy Decays and Microscale-Volume Viscometry Reveal the Compaction of Ribosome-Bound Nascent Proteins. *The Journal of Physical Chemistry B* **125**, 6543-6558 (2021).

- J. Lu, C. Deutsch, Secondary Structure Formation of a Transmembrane Segment in Kv Channels. *Biochemistry* 44, 8230-8243 (2005).
- 20. I. Mingarro, I. Nilsson, P. Whitley, G. Von Heijne, Different conformations of nascent polypeptides during translocation across the ER membrane. *BMC Cell Biol.* **1**, 3 (2000).
- 21. S. Bhushan *et al.*, α-Helical nascent polypeptide chains visualized within distinct regions of the ribosomal exit tunnel. *Nat. Struct. Mol. Biol.* **17**, 313 (2010).
- 22. C. A. Woolhead, P. J. McCormick, A. E. Johnson, Nascent membrane and secretory proteins differ in FRET-detected folding far inside the dribosome and in their exposure to ribosomal proteins. *Cell* **116**, 725-736 (2004).
- 23. X. Agirrezabala *et al.*, A switch from α-helical to β-strand conformation during cotranslational protein folding. *The EMBO Journal* **41**, e109175 (2022).
- 24. A. Kosolapov, C. Deutsch, Tertiary interactions within the ribosomal exit tunnel. *Nat. Struct. Mol. Biol.* **16**, 405-411 (2009).
- 25. O. B. Nilsson *et al.*, Cotranslational folding of spectrin domains via partially structured states. *Nat. Struct. Mol. Biol.* **24**, 221-225 (2017).
- 26. P. Tian *et al.*, Folding pathway of an Ig domain is conserved on and off the ribosome.

 *Proceedings of the National Academy of Sciences 115, E11284 (2018).
- 27. W. Holtkamp *et al.*, Cotranslational protein folding on the ribosome monitored in real time. *Science* **350**, 1104-1107 (2015).
- 28. M. Liutkute, M. Maiti, E. Samatova, J. Enderlein, M. V. Rodnina, Gradual compaction of the nascent peptide during cotranslational folding on the ribosome. *Elife* **9** (2020).

- G. Ziv, G. Haran, D. Thirumalai, Ribosome exit tunnel can entropically stabilize α-helices. *Proceedings of the National Academy of Sciences of the United States of America* 102, 18956 (2005).
- 30. J. Marino, G. von Heijne, R. Beckmann, Small protein domains fold inside the ribosome exit tunnel. *FEBS Lett.* **590**, 655-660 (2016).
- 31. M. Bañó-Polo *et al.*, Transmembrane but not soluble helices fold inside the ribosome tunnel. *Nature Communications* **9**, 5246 (2018).
- 32. F. Wruck *et al.*, The ribosome modulates folding inside the ribosomal exit tunnel.

 Communications Biology 4 (2021).
- 33. A. J. Samelson, M. K. Jensen, R. A. Soto, J. H. D. Cate, S. Marqusee, Quantitative determination of ribosome nascent chain stability. *Proceedings of the National Academy of Sciences of the United States of America* **113**, 13402-13407 (2016).
- 34. R. M. Addabbo *et al.*, Complementary Role of Co- and Post-Translational Events in De Novo Protein Biogenesis. *The Journal of Physical Chemistry B* **124**, 6488-6507 (2020).
- 35. S. Bhushan *et al.*, Structural basis for translational stalling by human cytomegalovirus and fungal arginine attenuator peptide. *Mol. Cell* **40**, 138-146 (2010).
- 36. G. Eisner, M. Moser, U. Schäfer, K. Beck, M. Müller, Alternate Recruitment of Signal Recognition Particle and Trigger Factor to the Signal Sequence of a Growing Nascent Polypeptide. *J. Biol. Chem.* 281, 7172-7179 (2006).
- 37. E. N. G. Houben, R. Zarivach, B. Oudega, J. Luirink, *Early encounters of a nascent membrane protein: specificity and timing of contacts inside and outside the ribosome* (2005), vol. 170, pp. 27-35.

- 38. J. H. Peterson, C. A. Woolhead, H. D. Bernstein, The conformation of a nascent polypeptide inside the ribosome tunnel affects protein targeting and protein folding. *Mol. Microbiol.* 78, 203-217 (2010).
- 39. R. S. Ullers *et al.*, Interplay of signal recognition particle and trigger factor at L23 near the nascent chain exit site on the Escherichia coli ribosome. *The Journal of cell biology* **161**, 679-684 (2003).
- 40. S. Bhushan *et al.*, SecM-stalled ribosomes adopt an altered geometry at the peptidyl transferase center. *PLoS Biol.* **9**, 10 (2011).
- 41. L. R. Cruz-Vera, S. Rajagopal, C. Squires, C. Yanofsky, Features of Ribosome-PeptidyltRNA Interactions Essential for Tryptophan Induction of tna Operon Expression. *Mol. Cell* **19**, 333-343 (2005).
- 42. H. Nakatogawa, K. Ito, The ribosomal exit tunnel functions as a discriminating gate. *Cell* **108**, 629-636 (2002).
- 43. B. Seidelt *et al.*, Structural Insight into Nascent Polypeptide Chain–Mediated Translational Stalling. *Science* **326**, 1412-1415 (2009).
- 44. B. Carragher *et al.*, Current outcomes when optimizing 'standard'sample preparation for single-particle cryo-EM. *Journal of microscopy* **276**, 39-45 (2019).
- 45. Y. Zhang, T. Wolfle, S. Rospert, Interaction of nascent chains with the ribosomal tunnel proteins Rpl4, Rpl17, and Rpl39 of Saccharomyces cerevisiae. *J. Biol. Chem.* **288**, 33697-33707 (2013).
- 46. C. Burridge *et al.*, Nascent chain dynamics and ribosome interactions within folded ribosome-nascent chain complexes observed by NMR spectroscopy. *Chemical Science* **12**, 13120-13126 (2021).

- 47. C. A. Waudby, C. Burridge, J. Christodoulou, Optimal design of adaptively sampled NMR experiments for measurement of methyl group dynamics with application to a ribosome-nascent chain complex. *J. Magn. Reson.* **326** (2021).
- 48. V. Guzman-Luna, A. M. Fuchs, A. J. Allen, A. Staikos, S. Cavagnero, An intrinsically disordered nascent protein interacts with specific regions of the ribosomal surface near the exit tunnel. *Communications biology* **4**, 1-17 (2021).
- 49. A. M. Knight *et al.*, Electrostatic Effect of the Ribosomal Surface on Nascent Polypeptide Dynamics. *Acs Chemical Biology* **8**, 1195-1204 (2013).
- 50. L. D. Cabrita *et al.*, A structural ensemble of a ribosome-nascent chain complex during cotranslational protein folding. *Nat. Struct. Mol. Biol.* **23**, 278-285 (2016).
- 51. L. D. Cabrita, S. T. D. Hsu, H. Launay, C. M. Dobson, J. Christodoulou, Probing ribosome-nascent chain complexes produced in vivo by NMR spectroscopy. *Proceedings* of the National Academy of Sciences of the United States of America 106, 22239-22244 (2009).
- 52. S. T. D. Hsu, L. D. Cabrita, P. Fucini, J. Christodoulou, C. M. Dobson, Probing Side-Chain Dynamics of a Ribosome-Bound Nascent Chain Using Methyl NMR Spectroscopy. *J. Am. Chem. Soc.* **131**, 8366-+ (2009).
- 53. A. R. Subramanian, B. D. Davis, R. J. Beller (1969) The ribosome dissociation factor and the ribosome-polysome cycle. in *Cold Spring Harbor symposia on quantitative biology* (Cold Spring Harbor Laboratory Press), pp 223-230.
- 54. R. J. Beller, B. D. Davis, Selective dissociation of free ribosomes of Escherichia coli by sodium ions. *J. Mol. Biol.* **55**, 477-485 (1971).

- 55. I. S. Edelman, P. O. Ts'o, J. Vinograd, The binding of magnesium to microsomal nucleoprotein and ribonucleic acid. *Biochimica et Biophysica Acta* **43**, 393-403 (1960).
- 56. P. T. Van Der Saag, J. M. Vlak, T. F. De Greef, Ribosomes from Xenopus laevis eggs and embryos in a cell-free protein-synthesizing system: translational regulation. *Cell Differentiation* 4, 385-397 (1976).
- 57. E. Z. Ron, R. E. Kohler, B. D. Davis, Magnesium ion dependence of free and polysomal ribosomes from Escherichia coli. *J. Mol. Biol.* **36**, 83-89 (1968).
- 58. J. Oppenheim, J. Scheinbuks, C. Biava, L. Marcus, Polyribosomes in Azotobacter vinelandii: I. Isolation, characterization and distribution of ribosomes, polyribosomes and subunits in logarithmically growing Azotobacter. *Biochimica et Biophysica Acta (BBA) Nucleic Acids and Protein Synthesis* **161**, 386-401 (1968).
- 59. W. S. Kelley, M. Schaechter, Magnesium ion-dependent dissociation of polysomes and free 70 s ribosomes in Bacillus megaterium. *J. Mol. Biol.* **42**, 599-602 (1969).
- 60. R. J. Beller, N. H. Lubsen, Effect of polypeptide chain length on dissociation of ribosomal complexes. *Biochemistry* **11**, 3271-3276 (1972).
- 61. A. S. Spirin, Structural transformations of ribosomes (dissociation, unfolding and disassembly). *FEBS Lett.* **40**, S28-S37 (1974).
- 62. P. Spitnik-Elson, B. Greeman, R. Abramovitz, The Influence of 6-M Urea on 30-S Ribosomes of Escherichia coli. *Eur. J. Biochem.* **49**, 87-92 (1974).
- 63. M. E. Roberts, I. O. Walker, Structural studies on Escherichia coli ribosomes: III.

 Denaturation and sedimentation of ribosomal subunits unfolded in urea. *Biochimica et Biophysica Acta (BBA) Nucleic Acids and Protein Synthesis* **199**, 184-193 (1970).

- 64. M. E. Roberts, I. Walker, Structural studies on Escherichia coli ribosomes: III.

 Denaturation and sedimentation of ribosomal subunits unfolded in urea. *Biochimica et Biophysica Acta (BBA)-Nucleic Acids and Protein Synthesis* **199**, 184-193 (1970).
- 65. A. Ilari, A. Bonamore, A. Farina, K. A. Johnson, A. Boffi, The X-ray structure of ferric Escherichia coli flavohemoglobin reveals an unexpected geometry of the distal heme pocket. *J. Biol. Chem.* **277**, 23725-23732 (2002).
- 66. A. Bonamore, A. Boffi, Flavohemoglobin: Structure and reactivity. *Iubmb Life* **60**, 19-28 (2008).
- 67. M. T. Forrester, M. W. Foster, Protection from nitrosative stress: A central role for microbial flavohemoglobin. *Free Radical Biol. Med.* **52**, 1620-1633 (2012).
- 68. K. Moncoq *et al.*, The PIR domain of Grb14 is an intrinsically unstructured protein: implication in insulin signaling. *FEBS Lett.* **554**, 240-246 (2003).
- 69. J. M. Beechem, E. Gratton, "Fluorescence spectroscopy data analysis environment: a second generation global analysis program" in Time-Resolved Laser Spectroscopy in Biochemistry, J. R. Lakowicz, Ed. (SPIE, Bellingham, 1988), 10.1117/12.945370, pp. 70-81.
- 70. D. M. Jameson, E. Gratton, R. D. Hall, The measurement and analysis of heterogeneous emissions by multifrequency phase and modulation fluorometry. *Appl. Spectrosc. Rev.* **20**, 55-106 (1984).
- J. A. Ross, D. M. Jameson, Time-resolved methods in biophysics. 8. Frequency domain fluorometry: applications to intrinsic protein fluorescence. *Photochem. Photobiol. Sci.* 7, 1301-1312 (2008).

- 72. S. A. Weinreis, J. P. Ellis, S. Cavagnero, Dynamic fluorescence depolarization: a powerful tool to explore protein folding on the ribosome. *Methods* **52**, 57-73 (2010).
- 73. M. M. Santoro, D. W. Bolen, Unfolding free-energy changes determined by the linear extrapolation method.1.unfolding of phenylmethanesulfonyl alpha-chymotrypsin using different denaturants. *Biochemistry* **27**, 8063-8068 (1988).
- 74. C. N. Pace, Measuring and increasing protein stability. *Trends Biotechnol.* **8**, 93-98 (1990).
- 75. G. Hermanson (2013) Bioconjugate techniques, Third edit. (Elsevier).
- 76. D. t. Hoare, D. Koshland, A method for the quantitative modification and estimation of carboxylic acid groups in proteins. *J. Biol. Chem.* **242**, 2447-2453 (1967).
- 77. R. N. Kirchdoerfer, J. J. T. Huang, M. K. Isola, S. Cavagnero, Fluorescence-based analysis of aminoacyl- and peptidyl-tRNA by low-pH sodium dodecyl sulfate-polyacrylamide gel electrophoresis. *Anal. Biochem.* **364**, 92-94 (2007).
- 78. A. Deckert *et al.*, Structural characterization of the interaction of α-synuclein nascent chains with the ribosomal surface and trigger factor. *Proceedings of the National Academy of Sciences* **113**, 5012-5017 (2016).
- 79. A. Raine, M. Lovmar, J. Wikberg, M. n. Ehrenberg, Trigger factor binding to ribosomes with nascent peptide chains of varying lengths and sequences. *J. Biol. Chem.* **281**, 28033-28038 (2006).
- 80. L. Ferbitz *et al.*, Trigger factor in complex with the ribosome forms a molecular cradle for nascent proteins. *Nature* **431**, 590-596 (2004).
- 81. S. K. Lakshmipathy *et al.*, Identification of nascent chain interaction sites on trigger factor. *J. Biol. Chem.* **282**, 12186-12193 (2007).

- 82. S. D. Lewis, J. A. Shafer, Conversion of exposed aspartyl and glutamyl residues in proteins to asparaginyl and glutaminyl residues. *Biochimica et Biophysica Acta (BBA) Protein Structure* **303**, 284-291 (1973).
- 83. F. U. Hartl, A. Bracher, M. Hayer-Hartl, Molecular chaperones in protein folding and proteostasis. *Nature* **475**, 324-332 (2011).
- 84. V. R. Agashe *et al.*, Function of trigger factor and DnaK in multidomain protein folding: increase in yield at the expense of folding speed. *Cell* **117**, 199-209 (2004).
- 85. M. F. Mecha, R. B. Hutchinson, J. H. Lee, S. Cavagnero, Protein folding in vitro and in the cell: From a solitary journey to a team effort. *Biophys. Chem.* **287**, 106821 (2022).
- 86. S. A. Teter *et al.*, Polypeptide Flux through Bacterial Hsp70: DnaK Cooperates with Trigger Factor in Chaperoning Nascent Chains. *Cell* **97**, 755-765 (1999).
- 87. F. Wruck *et al.*, Protein Folding Mediated by Trigger Factor and Hsp70: New Insights from Single-Molecule Approaches. *J. Mol. Biol.* **430**, 438-449 (2018).
- 88. E. Deuerling, A. Schulze-Specking, T. Tomoyasu, A. Mogk, B. Bukau, Trigger factor and DnaK cooperate in folding of newly synthesized proteins. *Nature* **400**, 693-696 (1999).
- 89. C. K. Bakke, L. M. Jungbauer, S. Cavagnero, In vitro expression and characterization of native apomyoglobin under low molecular crowding conditions. *Protein Expression Purif.* **45**, 381-392 (2006).
- 90. M. D. Dalphin, A. J. Stangl, Y. Liu, S. Cavagnero, KLR-70: A Novel Cationic Inhibitor of the Bacterial Hsp70 Chaperone. *Biochemistry* **59**, 1946-1960 (2020).

- 91. M. Behrmann *et al.*, Requirements for the translocation of elongation-arrested, ribosome-associated OmpA across the plasma membrane of Escherichia coli. *J. Biol. Chem.* **273**, 13898-13904 (1998).
- 92. H. Donis-Keller, Site specific enzymatic cleavage of RNA. *Nucleaic Acid Research* 7, 179-192 (1979).

FIGURES

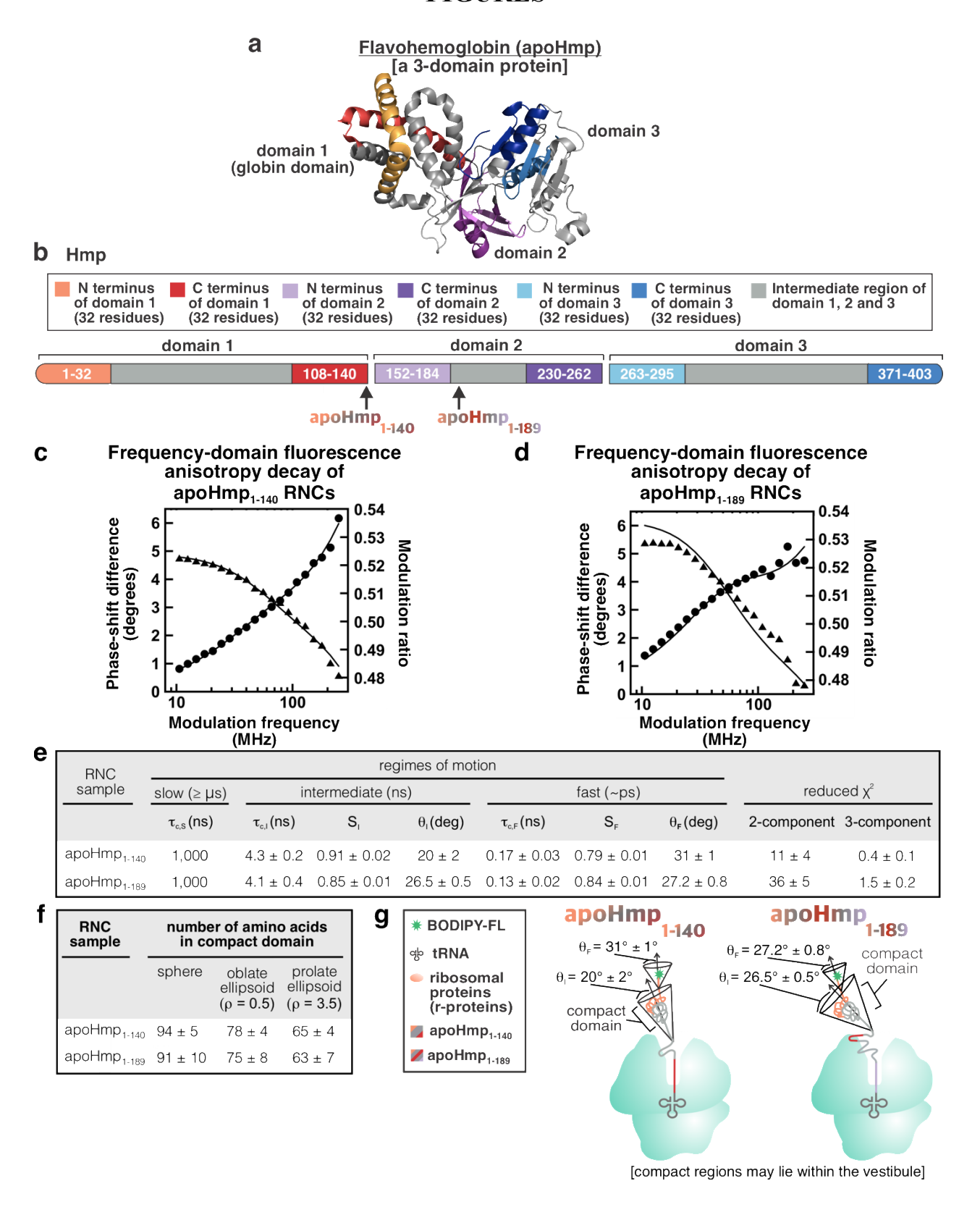


Figure 1. ApoHmp structure and and fluorescence-anisotropy decayed reveals compaction of apoHmp RNCs. a) *E. coli* flavohemoglobin (apoHmp) has three domains (shown in red, purple and blue). PDB code: 1GVH. b) Scheme illustrating the three domains of apoHmp and their corresponding N-and C-termini. Representative frequency-domain fluorescence anisotropy decay data for c) apoHmp1-140 and d) apoHmp1-189 RNCs. e) Table summarizing anisotropy decay parameters including rotational correlation times (rc), order parameters (S) and cone semi-angles (8). The S,I, and F subscripts denote slow-, intermediate-, and fast- timescale motions, respectively. Uncertainties are reported as \pm SE for n=3-5. Three-component anisotropy fits were selected as best fits if they led to a 2.5-fold decrease in reduced χ^2 , relative to two-component fits. The χ^2 of the chosen model is shown in bold. f) Table summarizing the number of amino acids comprising the RNC compact region, deduced from the rc,I rotational correlation time and assuming spherical, oblate ellipsoid, or prolate ellipsoid nascent-chain shapes. The parameter p denotes the axial ratio. e) Cartoon representation of apoHmp1-140 and apoHmp1-189 RNCs based on fluorescence anisotropy-decay data.

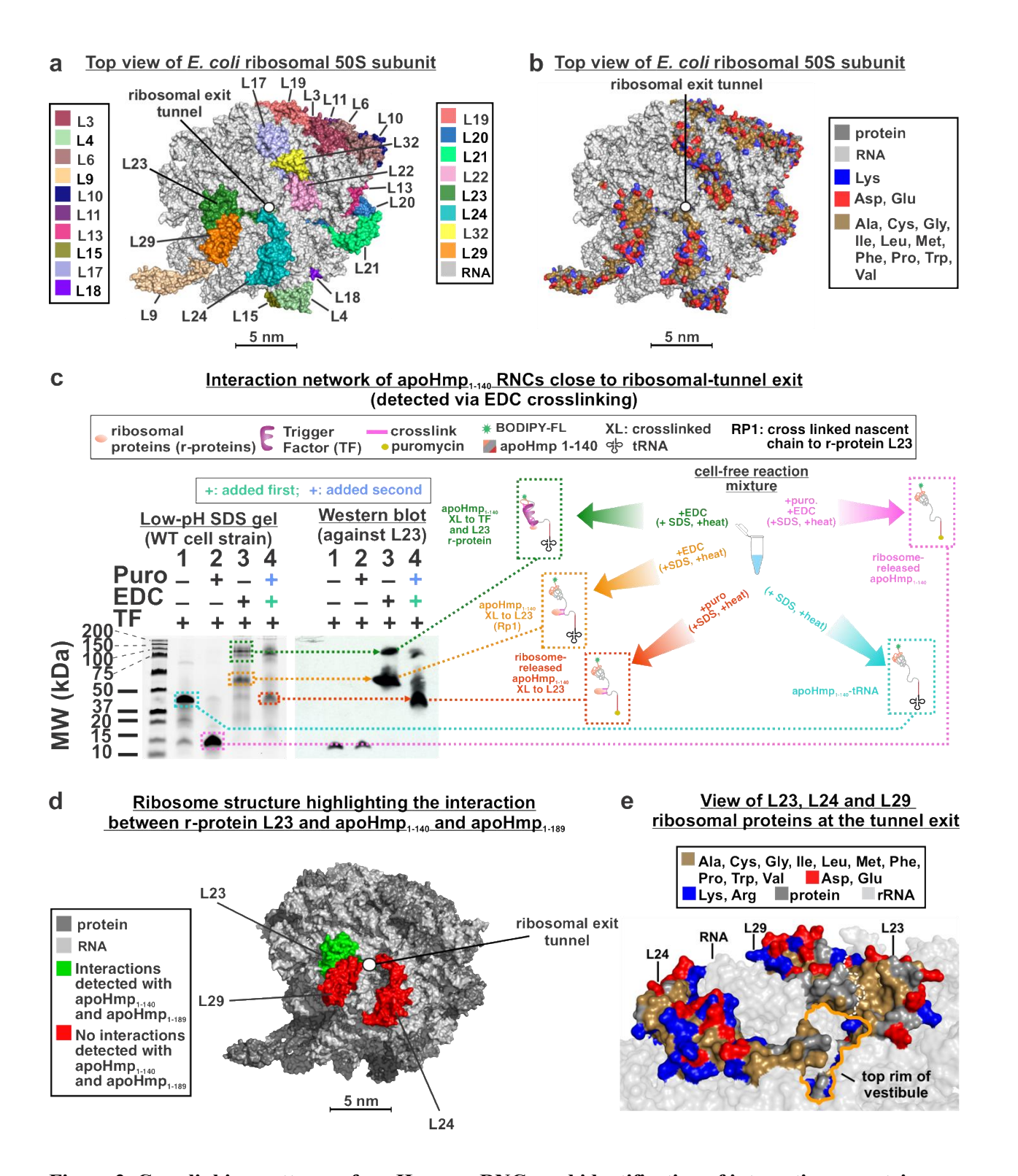


Figure 2. Crosslinking patterns of apoHmp₁₋₁₄₀ RNCs and identification of interacting r-proteins.

a) Top view of 50S subunit of the *E. coli* ribosome highlighting the ribosomal proteins (r-proteins).

Figure has been modified from (1) under a Creative Commons Attribution 4.0 International license. b)

Top view of 50S *E. coli* ribosome highlighting r-protein charged and nonpolar residues. Figure has been modified from *Guzman*, *et. al* under a Creative Commons Attribution 4.0 International license. **c)** SDS-PAGE and Western blot data identifying r-proteins interacting with apoHmp₁₋₁₄₀ RNCs in the absence and presence of the EDC crosslinker and the ribosome-release agent puromycin. Data show that the L23 r-protein interacts with apoHmp₁₋₁₄₀ RNCs. Corresponding data employing antibodies against L24 and L29 r-proteins, showing no interactions, are available in the SI Appendix. **d)** Top view of *E. coli* 50S ribosomal subunit highlighting the r-proteins that either interact (green) or do not interact (red) with apoHmp₁₋₁₄₀ and apoHmp₁₋₁₈₉ RNCs. **e)** Side view of r-proteins near the vestibule of the ribosomal exit tunnel. Figure has been modified from *Guzman*, *et. al.* under a Creative Commons Attribution 4.0 International license.

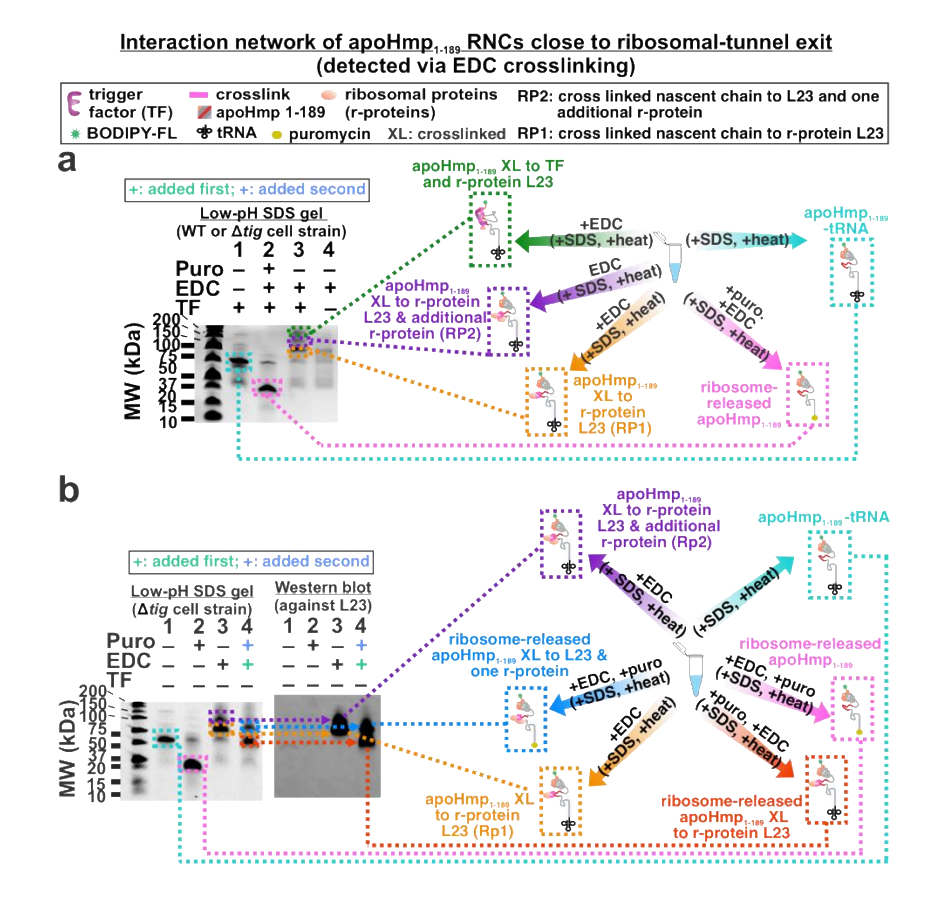


Figure 3. Crosslinking patterns of apoHmp₁₋₁₈₉ RNCs and identification of interacting proteins. a) Low-pH SDS-PAGE analysis of apoHmp₁₋₁₈₉ RNCs in the absence and presence of the EDC crosslinker, TF chaperone and the RNC ribosome-release agent puromycin. b) Side-by-side SDS-PAGE and Western blot data identifying the interaction network of apoHmp₁₋₁₈₉ RNCs in the absence and presence of EDC, puromycin and TF chaperone. The L23 r-protein is found to interact with apoHmp₁₋₁₈₉ RNCs.

Corresponding data employing antibodies against L24 and L29 r-proteins, showing no interactions, are available in the SI Appendix.

Urea sensitivity of nascent chain and RNC/-r-protein and RNC/chaperone complexes

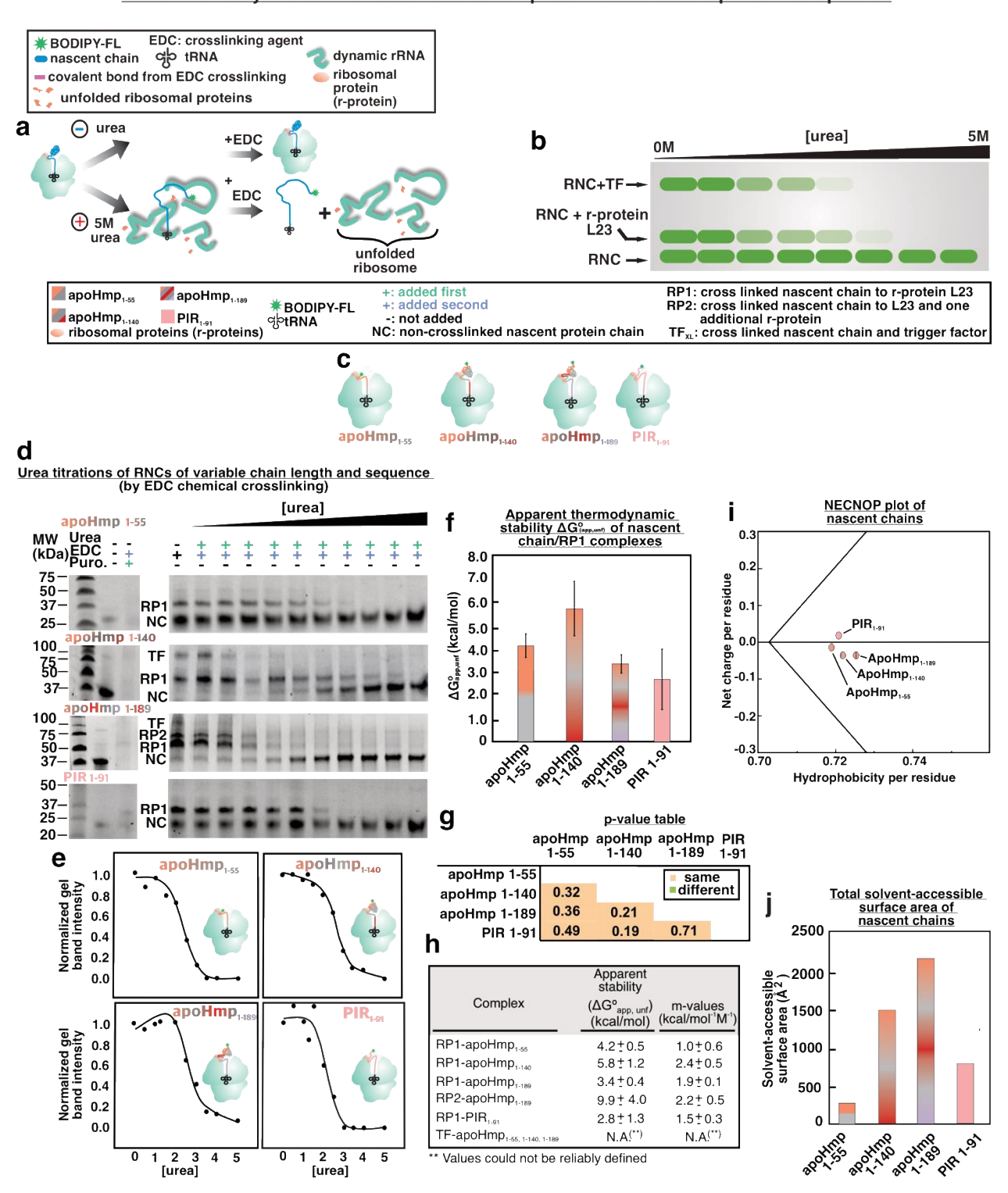


Figure 4. EDC-crosslinking-detected urea titrations showing the apparent stability of

RNC/-r-protein complexes. a) Scheme showing the expected effect of urea addition on RNCs

and b) corresponding low-pH SDS-PAGE gels. c) Four RNCs were tested in these experiments:apoHmp₁₋₅₅, apoHmp₁₋₁₄₀, apoHmp₁₋₁₈₉ or PIR₁₋₉₁. Note that PIR₁₋₉₁ is an intrinsically disordered protein (IDP). d) Representative SDS-PAGE analysis. Gel bands are reporters of the apparent stability of RNCs complexes with either L23 or TF. e) Representative urea titrations of apoHmp₁₋₅₅, apoHmp₁₋₁₄₀, apoHmp₁₋₁₈₉ and PIR complexes. f) ΔG° app,unfold values in the presence of low concentrations of chaperones (2-15 nM of TF and 0.5 μ M, 0.04 μ M and 0.05 μ M of and DnaK, DnaJ and GrpE respectively). Uncertainties are reported as \pm SE for n=2-3. g) P-value table for a two-tailed Student's Ttest, comparing the ΔG°app, unfold values of RNC/r-protein complexes. Green and orange boxes denote statistically different and statistically equivalent data, respectively, according to a 95% confidence interval. h) Table displaying relevant ΔG° app, unfold and m-values. i) NECNOP plot (100) displaying net charge/residue as a function of hydrophobicity/residue of PIR1-91, apoHmp1-55, apoHmp1-140, apoHmp1-189 protein chains. i) Estimated total solvent-accessible surface areas of protein chains. assuming fully extended conformations. Values were computed with Surfracer (101).

<u>Urea sensitivity of RNC/-r-protein and RNC/chaperone complexes at low and high chaperone concentrations</u> (detected via EDC crosslinking)

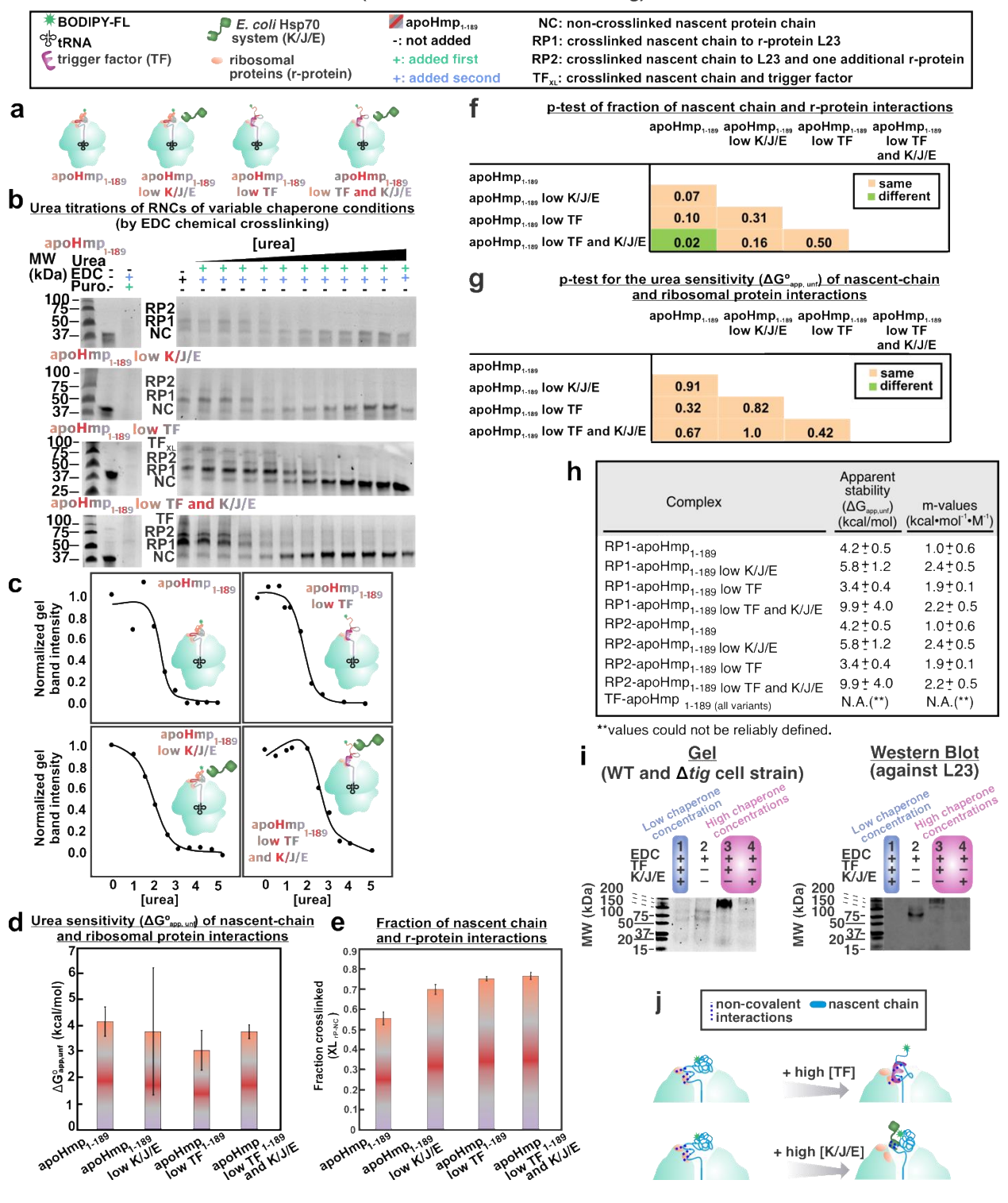


Figure 5. Low pH SDS-PAGE and urea-titration analysis of ApoHmp₁₋₁₈₉ in the absence and presence of TF and K/J/E chaperones. a) Cartoon illustrating the tested RNCs. b) Low pH SDS-PAGE analysis of complexes including apoHmp₁₋₁₈₉ RNC and either r-proteins or molecular chaperones as a function of increasing urea concentration. c) Representative urea titration curves. d) $\Delta G^{\circ}_{app,unfold}$ values in the absence and presence of low concentrations (2-15 nM of TF and 0.5 μM, 0.04μM and 0.05μM of and DnaK, DnaJ and GrpE respectively) of molecular chaperones. Error bars denote standard error based on 2-3 experiments. e) Fraction of RNC/r-protein complexes relative to total RNCs. Uncertainties are reported as \pm SE for n=2-3. f) P-value table for two-tailed Student's test assuming unequal variances, comparing $\Delta G^{\circ}_{app,unfold}$ values. Green and orange boxes denote statistically different and statistically equivalent data, respectively, according to a 95% confidence interval. g) P-value table comparing fractions of RNC/r-protein complexes. Statistical assessments were similar to those listed in panel f. h) Table showing ΔG° app,unfold and m values of relevant complexes. i) Low-pH SDS-PAGE analysis of apoHmp₁₋₁₈₉ RNCs treated with EDC in the absence and presence of chaperones at low (lanes 1 and 2, (2-15 nM of TF and 0.5 μM, 0.04μM and 0.05μM of and DnaK, DnaJ and GrpE respectively) and higher concentrations (8 μM for TF and 10/2/4 μM for K/J/E respectively, lanes 3 and 4). Western Blot analysis probing interactions with ribosomal protein L23. j) Schematic representation of RNC interaction networks at low (2-15 nM of TF and 0.5 μM, 0.04μM and 0.05μM of and DnaK, DnaJ and GrpE respectively) and higher (8 μM and 10/2/4 μM K/J/E, respectively) chaperone concentrations.

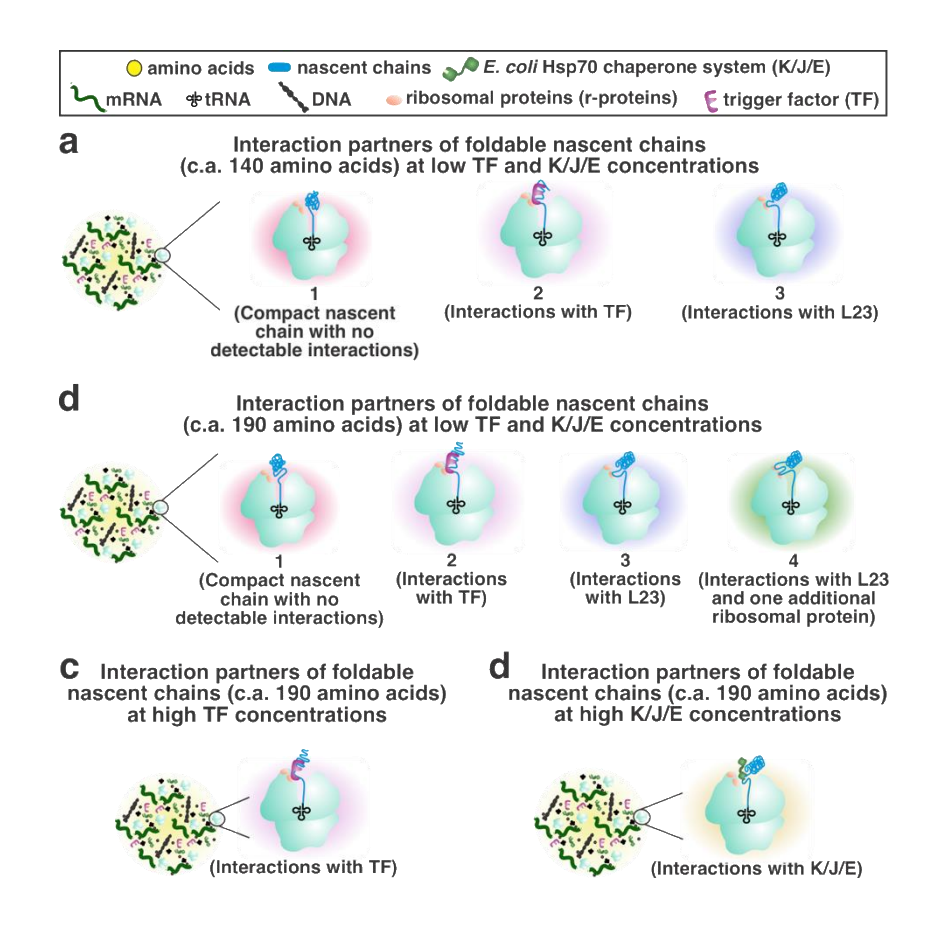


Figure 6. Cartoon summarizing the RNC interaction networks detected in this work under different experimental conditions. Interaction partners of a) apoHmp₁₋₁₄₀ and b) apoHmp₁₋₁₈₉ RNCs at low chaperone concentrations (2-15 nM of TF and 0.5 μ M, 0.04 μ M and 0.05 μ M of and DnaK, DnaJ and GrpE respectively). c) Interaction partners of apoHmp₁₋₁₈₉ RNCs at higher c) TF (8 μ M) and d) K/J/E chaperone concentrations (10/2/4 μ M K/J/E, respectively).

SI APPENDIX

Nascent-Chain Interaction Networks and Their Effect on the Bacterial Ribosome

Meranda M. Masse^a, Valeria Guzman-Luna^a, Angela E. Varela^{a,+}, Rachel B. Hutchinson^a, Aniruddha Srivastava^{a,‡}, Wanting Wei^{a°,} Andrew M.Fuchs^a and Silvia Cavagnero^a*

Department of Chemistry, University of Wisconsin-Madison, Madison, Wisconsin, 53706,
 USA.

Present Address

- ⁺A.E.V.: School of Veterinary Medicine, University of Wisconsin-Madison, Madison, Wisconsin, 53706, USA.
- [‡] A.S.: School of Medicine and Public Health, University of Wisconsin-Madison, Madison, Wisconsin, 53705, USA.
- ° W.W.: AIDS Vaccine Research Laboratory, University of Wisconsin-Madison, Madison, Wisconsin, 53711, USA.

Corresponding Author

* Email: cavagnero@chem.wisc.edu. Phone: 608-262-5430

SUPPORTING TEXT

Sucrose-gradient analysis of 70S empty ribosomes and ribosome-peptidyl-tRNA complexes.

In order to explore the effect of nascent-chain characteristics on the bacterial ribosome, we examined whether the incorporation of aminoacyl initiator tRNA (Met-tRNA fMet) or very short peptidyl tRNAs affects the ribosomal complex in the presence of urea. We collectively denote these species, which were generated via oligodeoxynucleotide-directed mRNA cleavage (2-4) (see Methods), as tRNAs carrying short nascent chains, or snc-tRNAs. Note that the antisense DNA construct used in the oligonucleotide-directed mRNA cleavage approach was designed to generate ribosome stalling after the first N-terminal residue (Met) of the nascent chain only. It is known that the E. coli RNAse H enzyme, employed here in conjunction with antisense oligodeoxynucleotides, typically establishes well-defined sharp cleavage sites, characterized by a site-specific distribution of the cleavage site of ca. 1-3 nucleotides (4). Hence a dominant population of very short (1-3 residues) nascent chains in the ribosomal complexes encompassing snc-tRNAs is expected, consistent with the observed sharp gel bands (SI Appendix, Fig. S1). It follows that the nascent chains belonging to snc-tRNAs are not sufficiently long to interact with ribosomal proteins (r-proteins) across the ribosomal exit tunnel (5). In addition, the specific thermodynamic stabilization imparted by RNA-oligodeoxynycleotide complexation was designed to be at least 12.4 kcal/mole, with a corresponding antisense-oligodeoxynucleotide length ranging from 11 to 38 DNA bases. The above free-energy value is significantly larger than what was used in the original report of the oligodeoxynucleotide-directed RNA cleavage approach (4). Therefore, ribosomal complexes that include snc-tRNAs are expected to bear no contributions due to interactions of nascent chains with ribosomal proteins. It is worth noting, however, that in the case of some specific RNA sequences under non-optimal conditions, the cleavage-site distribution

width was found to be larger than 1-2 residues (6). Therefore, in our case, any hypothetical longer RNCs than 1-3 residues are expected to be poorly populated.

Once appropriate RNCs harboring snc-tRNAs were made, we set out to test the response of the ribosome against exposure to urea. Specifically, we compared the urea sensitivity of empty 70S ribosomes (SI Appendix, Fig. S1a-b) to that of ribosomes harboring snc-tRNAs (SI Appendix Fig. S1c) by sucrose gradient-detected urea titrations. Sucrose gradients are able to resolve ribosomal subunits and entire 70S ribosomal particles (7). Further, these gradients have previously been employed to monitor the unfolding of whole ribosomes or ribosomal subunits in the absence and presence of targeted structure-perturbing buffers (8-15) (e.g., containing EDTA or other related agents) or classical denaturing agents like urea.(16-18) Conveniently, high concentrations of urea do not perturb elution-profile integrity through line-broadening or other effects. (19) Therefore, urea titrations of the 70S ribosome including sucrose-gradient detection are a powerful tool to explore ribosomal-subunit dissociation and unfolding.

Sucrose-gradient elution profiles were monitored at 260 (SI Appendix Fig. S1) and 280 nm (SI Appendix, Fig. S3) in separate experiments, to probe for any potential differences in the response of rRNA and r-proteins. Our data show that rRNA and r-proteins belonging to 70S ribosomal particles devoid of tRNA and nascent chains, denoted here as empty ribosomes, are overall stable up to 1.0 M urea, with only a small extent of dissociation of the 70S particle into its 30S and 50S subunits (SI Appendix Fig. S1a). At 2 M urea, empty ribosomes undergo subunit dissociation accompanied by extensive line-broadening. Due to the dominant presence of intact 16S and 23S rRNA band in ethidium bromide-stained agarose gels (SI Appendix Fig. S2), line broadening is not ascribed to rRNA degradation. Therefore, we interpret the broad sucrose-gradient peaks observed at 2 M urea as diagnostic of rRNA and(or) r-protein unfolding

accompanied by conformational heterogeneity. At > 2 M urea, both the empty ribosome, and ribosomes harboring snc-tRNA undergo severe line-broadening (SI Appendix Fig. S1). At the highest urea concentration tested in this work (4 M), line-broadening is so extensive that it is difficult to deconvolute the contribution of individual ribosomal components. A similar scenario is supported by the empty-ribosome data at 280 nm, suggesting that rRNA and r-protein unfolding proceeds in concert (SI Appendix Fig. S3).

Ribosomes carrying tRNAs linked to very short nascent chains (snc-tRNA) are also characterized by progressive disassembly, as urea concentration increases (SI Appendix Fig. S1 and S3). Unlike empty ribosomes, however, the ribosomes harboring snc-tRNAs are still ca. 50% intact at 2 M urea. Further, at this urea concentration the 30S and 50S subunits (dissociated from 70S intact ribosomes) have not yet undergone any unfolding, given that no line broadening is observed.

Notably, the sucrose gradient profiles of ribosomes harboring snc-tRNAs also display two additional peaks eluting after the 70S ribosome (SI Appendix Fig. S1 and S3). These features are either due to polysomes (i.e., nearby ribosomes linked via the same mRNA strand) or to self-associated ribosomes brought together by through-space noncovalent surface contacts. The mRNA encoding short nascent-chains (sncs) is predominantly cleaved only 11 ribonucleotides away from the mRNA ribosome binding site, i.e. the Shine-Dalgarno sequence (20). Ribosome profiling (21) and structural considerations reveal that each translating bacterial ribosome spans a length corresponding ca. 24 ribonucleotides (22). Further, computer simulations suggested that polysomes have c.a. 24 residues between neighboring ribosomes (23). Therefore, geometrical factors render polysome formation very unlikely. To gain further insights, transmission electron microscope (TEM) negative stain images of ribosomes carrying snc-tRNAs were acquired in the

presence of 2% methyl-tungstate (24). The representative TEM image displayed in Figure 3 shows that, in addition to isolated ribosomes (within dashed blue squares), some closely spaced ribosomes (within dashed red squares) comprising 2 or more particles are also present. The spatial arrangement of these particles renders it impossible to establish where these species are polysomes or other forms of self-associated ribosomes. While polysomes seem unlikely due to the above-listed geometrical arguments, it is possible that some longer-than expected nascent chains may be populated in these samples, preventing the ruling out of polysomes. In all, the origin of the late-eluting peaks found in ribosome samples harboring snc-tRNAs remains unestablished and further future investigations are required to shed further light on this matter. On the other hand, the disassembly pattern of these peaks is entirely like that of 70S ribosomes harboring snc-tRNAs. Therefore, the late-eluting peaks do not add any new information nor modify the conclusions reached for the 70S particles.

The urea sensitivity of a representative ribosome harboring a longer nascent chain (32-residue long) derived from *E. coli* Hmp₁₀₈₋₁₄₀ has also been analyzed. The results are shown in Figure 4 and SI-Appendix Figure S3. These ribosomes behave in the same way as ribosomes harboring snc-tRNAs, suggesting that nascent-chain length does not affect the apparent stability of the 70S ribosome, and that the enhanced apparent stability may be dominated by the role of the tRNA. Additional experiments probing this topic in further detail are described in some sections of the main manuscript.

In summary, the data in SI Appendix Figures 1-3 show that empty-intact 70S ribosomes are more sensitive to urea-induced denaturation than ribosomes carrying tRNAs linked to nascent chains of variable lengths.

Nascent-chain sequence and length (beyond 32 residues) does not affect the PTC. Puromycin is a small-molecule antibiotic that induces premature release of nascent polypeptides from the ribosome. It mimics the adenosine-Phe portion of the CCA 3' end of Phe-tRNA^{Phe} (SI Appendix, Fig. S5). Puromycin gets incorporated into nascent polypeptides as a result of nucleophilic attack of the carboxyl C -terminus of the nascent chain (25). On the other hand, this antibiotic works properly only if the A and P sites, which are entirely located within the 50S subunit, are intact (26). At high urea concentrations, the PTC is denatured and puromycin is no longer able to promote the release of nascent protein chains from the ribosome.

The main features of the puromycin ribosome-release assay and its urea-concentration dependence are illustrated in SI Appendix Figure 5a, b. In short, RNC reactivity to puromycin is monitored via low-pH gels (27) as a function of increasing urea concentration.

We performed low-pH SDS-PAGE analysis on a variety of apoHmp RNCs comprising variable chain-length values (SI Appendix, Fig. S5), net charge and hydrophobicity, and degree of folding. The target nascent protein chains included snc (i.e., a 1-3 amino acid chain derived from apoHmp), apoHmp₁₋₃₂, apoHmp₁₀₈₋₁₄₀, apoHmp₁₋₁₄₀ and apoHmp₁₋₁₈₉. These constructs specifically enabled us to probe differences between nascent-chain sequences located within the ribosomal exit tunnel core, as well as partially and fully folded nascent-chain domains. Low-pH SDS-PAGE was used to generate peptidyl tRNA (PT) bands whose intensities were quantified as a function of increasing urea concentration. The peptidyl-puromycin band (PP) was not used to track ribosome release because of its highly environmentally sensitive fluorescence intensity. Titration curves were generated based on the relative band intensities of the PT bands of each construct, reporting on the extent of puromycin reactivity (SI Appendix Fig. S5c). The data were then fit to an equation relating the experimental observable at variable urea concentrations to the apparent stability

 $(\Delta G^{\circ}_{app, unfold})$ of each construct, following the general procedures by Santoro and Bolen (28, 29) (see Methods).

As shown in SI Appendix Figure S5d-f, the results indicate that the apparent stability of the PTC center, monitored via puromycin activity assays, is very similar for all nascent-chain construct. Moreover, the two-tailed Student's test assuming unequal variances (Welch's test) shows that most constructs display equivalent behavior (SI Appendix Fig. S5f). In other words, most constructs contribute to a similar extent to the apparent stability of the PTC, amounting to ca. 2.5 – 4.5 kcal/mol. Therefore, the urea sensitivity of the PTC does not depend on nascent-chain properties. and may be dominated by the stabilizing effect of the tRNA. The results also suggest that the specific tRNA sequence does not have an effect either. An exception is provided by snc and apoHmp₁₋₁₄₀ nascent proteins, given that the apoHmp₁₋₁₄₀ construct displays a statistically significant PTC-stabilizing role. This feature is likely not due to the compact partially folded state of apoHmp₁₋₁₄₀, given that fluorescence anisotropy shows that nascent apoHmp₁₋₁₈₉ has a comparable degree of compaction.

Note that ribosome disassembly and unfolding due to denaturing agents is an irreversible process (30). Therefore, true thermodynamic $\Delta G^{\circ}_{unfold}$ values cannot be obtained, upon treating the ribosome with denaturing agents. Thus, we refer to the $\Delta G^{\circ}_{unfold}$ values derived in this and the following sections of this work as *apparent stability* values. The mere function of these quantities, which were derived from data fitting of urea-titrations, is to describe the urea sensitivity – and not the thermodynamic stability – of specific portions of *E. coli* ribosomes.

Sequence of events leading to ribosome disassembly: role of tRNA and nascent proteins. Finally, a proposed equilibrium ribosome disassembly mechanism based on the data of SI Appendix Figures 1 through 5 is shown in SI Appendix Figure S8. The simple steps displayed in

panel a of SI Appendix Figure S8 pertain to empty 70S ribosomes and are consistent with the sucrose gradient data. The ribosome starts disassembling into its component 50S and 30S subunits at 1 M urea. More extensive subunit disassembly together with subunit unraveling follows at higher urea concentrations. This process is accompanied by pervasive r-protein and rRNA conformational heterogeneity, likely due to disruption of secondary and tertiary structure leading to r-RNA and r-protein unfolding. Panel b of the same figure shows how the process gets modified if the ribosome carries aminoacyl or peptidyl tRNA. Briefly, in this case the ribosomal-subunit disassembly occurs at higher urea concentrations (1 -2 M). Given the weak dependence of the sucrose-gradient and puromycin assays on the nature of the nascent chain, we deduce that the tRNA likely dominates the effect and that the length, hydrophobicity, net charge and foldability of apoHmp nascent chains do not play a stabilizing role in ribosome stability.

SUPPORTING MATERIALS AND METHODS

Denaturation of ribosome-nascent-chain complexes and empty ribosomes. A 10 M stock solution of 0.22 μm-filtered urea was prepared in resuspension buffer and the refractive index was measured with an Abbe Refractometer (Thermo Spectronic, Fisher Scientific) to derive actual urea concentrations as described (31). RNCs subject to sucrose cushion ultracentrifugation (see section on RNC preparation) or empty ribosomes obtained from crude S30 were incubated in the presence of variable concentrations of urea for 1 hr at ambient temperature in the dark.

Assessment of urea sensitivity of 70S ribosome and RNCs via sucrose gradient analysis. An in-house prepared A19 *E. coli* mixture (with 70S ribosomes) was incubated for 1 hr at variable urea concentrations at ambient temperature. Samples were loaded onto a 5-45% sucrose gradient and centrifuged using a Beckman L-70 Ultracentrifuge with a SW41 rotor at 288, 000 x g for 1.5

hrs at 4 °C. Gradient profiles were obtained on a Biocomp Fractionator at 0.2 mm/sec. The absorbance was measured at 254 nm and 280 nm using a Triax flow cell from BioComp to check for intactness of the rRNA and r-proteins, respectively. RNCs were treated in a similar manner after denaturation in urea for 1 hr (see RNC denaturation in Methods). The 30S, 50S and 70S subunits were collected in both instances and loaded on a 2% agarose gel (0.02 M Tris Base, 0.01 M acetic acid and 0.0005 M EDTA, or 0.5x TAE). Ethidium bromide was added to a final concentration of 0.5 µg/mL. Samples were run for 100 min at 3.92 V/cm. The gel was imaged on a GE FLA 9500 Laser Imager at PMT values between 500-700.

Imaging of RNCs via negative staining. RNC samples prepared in the presence of Met-tRNA flower

(2 μL) were placed onto a glow-discharged copper 300-mesh formvar-carbon grid (made in house by Medical Sciences Electron Microscopy staff at UW-Madison), blotted with filter paper and allowed to dry. A Nano-W staining solution (Nanoprobes) was placed on the grid in equal volume, blotted with filter paper and allowed to dry. Images were collected on a CM120 transmission electron microscope (Philips) at 140000x magnification and 80 keV using a BIOSPR12 camera.

Assessment of apparent stability of RNC/-r-protein and RNC/chaperone complexes via a crosslinking assay. The EDC crosslinker is capable of capturing interactions involving RNCs and r-proteins or chaperones within the ribosomal exit-tunnel vestibule and outside the ribosomal exit-tunnel core (1). Either ribosome-bound or ribosome-released control samples (with EDC added after RNC ribosome release) were used to probe RNC production and to test the lack of ribosome-released nascent-chain crosslinking to other species. After incubation in urea for 1 hr, a 10x concentration of EDC solution (800 mM EDC, pH 6.8-7.0) was added to RNCs to a final concentration of 1x. Samples were incubated for 30 min at 30 °C and then quenched with a 10x concentration of Quenching Buffer (1.0 M Tris-HCl pH 7.0, 1.0 M Glycine, 1.0 M KOAc) to a

final concentration of 1x (0.1 M Tris-HCl pH 7.0, 0.1 M Glycine, 0.1M KOAc). Samples were loaded onto a low-pH SDS-PAGE gels using either a 10% acrylamide gel (apoHmp₁₋₅₅, apoHmp₁₋₁₄₀ and apoHmp₁₋₁₈₉) or a 9% acrylamide gel (PIR) in a 1:1 ratio with loading buffer. Gels ran at 3.92 V/cm for either 4 hours (apoHmp₁₋₅₅, apoHmp₁₋₁₄₀ and apoHmp₁₋₁₈₉) or 2.5 hrs (PIR) and were imaged on a GE FLA 9500 Laser Imager. Fluorophores were excited at 473 nm, with a PMT value within the 700-950 range.

Crosslinked band intensities were evaluated via the ImageJ software (32). The normalized intensity of each band was assessed via relation $I_{XL} = \frac{I_{1,XL}}{I_{2,XL}}$, where I_{XL} is the normalized intensity of an individual crosslinked species, $I_{1,XL}$ is the intensity of the individual crosslinked species, $I_{2,XL}$ is the intensity of the species at 0 M urea. The fractional band intensities were then plotted as a function of urea concentration and then plotted to fit pre- and post- transition region baselines. A 2-state unfolding expression taking pre- and post-transition baseline slopes into account (28) was used to fit the raw urea-titration data and deduce m-value and ΔG°_{H2O} values via the Kaleidagraph software (29).

Western Blot analysis of r-protein interactions with L23, L24 and L29. Western Blots were performed as described (1). Aliquots of the rabbit anti-uL23 antibody were kindly donated by Shu-ou Shan (California Institute of Technology). The anti-uL23 antibody was generated by GenScript, using the CGKVKRHGQRIGRRS peptide as epitope and has been validated in previous work (33). Rabbit anti-uL17, -uL18/L22, -uL24, -uL29, and -uL32 antibodies were kindly facilitated by Bryan W. Davies (University of Texas-Austin) and Melanie Oakes (University of California, Irvine) who obtained them from Masayasu Nomura (University of Wisconsin-Madison). The antibodies were generated using the purified *E. coli* ribosomal proteins L17, L23, L18+L22, L24, L29, and L32 (34).

Assessment of apparent stability of PTC via a puromycin-assisted nascent-chain release assay. To confirm that the polypeptide was attached to the ribosome, a low-pH SDS-PAGE(27) using a 9% acrylamide gel was conducted before (positive control) and after treatment of 1 mM puromycin, which reacted with the samples for 30 minutes at 37 °C. Samples were loaded on gels in a 1:1 ratio with loading buffer. Identical samples of the positive control and puromycin-released samples at 2.23 M urea were loaded on each gel to control for intrinsic gel differences (i.e., gel crosslinking, which may affect the fluorophore quantum yield). Prior to gel loading, samples were heated at 37 °C for five min and allowed to sit at room temperature for 5 min. Gels ran at 3.92 V/cm for 3.5 hr and imaged on a GE FLA 9500 Laser Imager. Fluorophores were excited at 473 nm and a PMT value between 315-700.

Due to the number of samples, 2 gels were needed for the positive control samples and 2 gels were needed for the puromycin-released samples per experiment. Fluorescence intensity adjustments were made between gels by normalizing the 2.23 M urea samples from each gel via Equation 1

$$I_{\text{intergel}} = \frac{I_{2.23 \text{ M urea,gel 1}}}{I_{2.23 \text{ M urea,gel 2}}} * I_{\text{x,gel 2}}$$
(S1)

where $I_{2.23 \text{ M urea, gel1}}$ and $I_{2.23 \text{ M urea, gel2}}$ refer to the band intensities of the 2.23 M urea sample in each gel. I_{gel2} is the band intensity of the sample loaded onto the second gel and $I_{x,intergel}$ is any given band intensity on the second gel in comparison to the band intensity of the first gel.

To control for differences in RNC concentrations and compare band intensities between the bound and released sample gels, Equation 2 was used

$$I_{\text{relative}} = \frac{I_{\text{+puro}}}{I_{\text{-puro}}},$$
 (S2)

where I +puro is the band intensity of the puromycin-released sample and I -puro is the band intensity of the positive control. Band intensities were then divided by the band intensity of the sample

containing the highest urea concentration to normalize intensities between 0 and 1. The resulting intensities were plotted to fit pre- and post- transition region baselines. Using an extrapolation method (28), the transition region slope and y-intercept were deduced to obtain the m-value and ΔG°_{H2O} with the Kaleidagraph software (29).

Ribosomal-protein (r-protein) stability assessment via a Trp fluorescence-emission assay. The *E. coli* r-proteins collectively contain 32 Trp residues. Trp is sensitive to changes in its environment and exposure to polar solvents causes a red-shift in its excitation spectra, which was monitored as a function of increasing urea concentrations (35-37). RNC samples were excited at 285 nm (bandpass of 4 nm) and the fluorescence was monitored from 295-500 nm (bandpass of 4 nm) on a Photon Counting Spectrofluorimeter (ISS) since the indole group of tryptophan is the major component of UV absorbance in that region (38).

To generate a titration curve for the RNC complex, the buffer spectra was first subtracted from the produced emission spectra. Then a baseline correction was done on the resulting spectra. The spectral center of mass of the resulting spectra was obtained using the emission spectra between 300-385 nm (to omit the scatter peak and Raman peak) and Equation 3

Spectral center of mass (nm) =
$$\frac{\Sigma(\lambda) \times I_{\lambda}}{\Sigma(I)}$$
, (S3)

where λ is the wavelength and I_{λ} is the intensity at a specific wavelength.

The fraction of unfolded protein at each concentration of urea was determined according to

$$\Delta \text{Fraction of unfolded ribosome} = \left(1 + Q\left(\frac{\lambda_{x} - \lambda_{\text{unfold}}}{\lambda_{\text{fold}} - \lambda_{x}}\right)\right)^{-1}, \quad (S4)$$

where λ_{fold} is the shortest wavelength calculated from Equation 3 for the folded species and λ_{unfold} is the longest wavelength calculated from Equation 3 for the unfolded species. Q denotes the ratio

between the quantum yields of folded and unfolded states. Quantum-yield changes were calculated by taking highest intensity values from each folded sample (0.0 M, 0.13 M and 0.45 M urea) as well as each unfolded sample (5.5 M, 6.0 M and 6.5 M urea). The three folded and unfolded values were averaged amongst their respective groups to determine Q. ΔCoM was plotted as a function of urea concentration and the pre- and post- transition baselines were determined in Microsoft Excel. Free energy of unfolding curves were generated with the software Kaleidagraph (Synergy Software) using a known extrapolation method.

SUPPORTING TABLES

Table S1. Summary of published experimental evidence on interactions between nascent protein chains (RNCs) and the ribosome based on single-particle cryo-EM or chemical crosslinking data.

Table S2. Name, nucleotide sequence, and calculated ΔG° of unfolding for each oligo nucleotide used in this work. ΔG° was calculated using an online calculator (biosyn.com). Sequences used for calculation are as shown.

SUPPORTING FIGURE LEGENDS

Figure S1. Sucrose gradient profiles for both empty 70S ribosomes (a), the same 70S ribosome profile is set to the same y-axis scale as the short (1-2 amino acid) nascent chains (snc-tRNA), (b) ribosomes harboring short (1-2 amino acid) nascent chains (c), ribosomes bearing a longer nascent-peptide chain (d), and the same ribosomes bearing a longer nascent-peptide chain at the full vertical scale (e) are shown for increasing concentrations of urea. Profiles were collected at 260 nm. (f) A TEM image of the snc-tRNA is shown. The dark blue squares show what are likely isolated 70S ribosomes and the red squares show closely spaced ribosomes.

(g) Bound and released snc-tRNA and apoHmp₁₋₁₄₀ nascent chains with the addition of puromycin (released) or without (bound) on a low pH 10% SDS-PAGE gel.

Figure S2. (a) The 70S bacterial ribosome contains two subunits, the 30S (blue) and the 50S (purple), which contain the 16S and 23S rRNA respectively. (b) Representative agarose gel stained with ethidium bromide for the 30S, 50S and 70S of ribosome samples at increasing concentrations of urea. Subunit peak corresponds to the area in which the sample was collected.

Figure S3. Sucrose gradient profiles for both empty 70S ribosomes (a), the same 70S ribosome profile is set to the same y-axis scale as the short (1-2 amino acid) nascent chains (b), and ribosomes harboring short (1-2 amino acid) nascent chains (c), ribosomes bearing a longer nascent-peptide chain (d), and the same ribosomes bearing a longer nascent-peptide chain at the full vertical scale (e) are shown for increasing concentrations of urea. Profiles were collected at 280 nm.

Figure S4.) E. coli flavohemoglobin (apoHmp) is the model foldable protein used in this study. apoHmp has three domains (shown in red, purple and blue). PDB code: 1GVH. b) The phosphorylated insulin receptor interacting region of the Grb14 protein from rat (PIR) is the model intrinsically disordered protein used in this work. c) A pictorial representation of the three domains of ApoHmp and their corresponding N-and C-termini are shown. d) The pictorial sequence length of PIR is shown to scale. e) Eleven constructs were derived from apoHmp to determine whether nascent chain length or sequence had any effect on the stability of r-proteins, and four representative constructs were chosen to assess peptidyl-transferase center (PTC) site stability. The construct denoted "snc-tRNA" had a nascent chain length of one to three amino acids that were used to determine the relative contribution of tRNA to the stability of the ribosomal complex. apoHmp₁₀₈₋₁₄₀, apoHmp₁₋₃₂, apoHmp₂₃₀₋₂₆₂, apoHmp₁₅₂₋₁₈₄, apoHmp₃₇₁₋₄₀₃ and apoHmp₂₆₃₋₂₉₅ denoted constructs contained either the N- or C- termini of the respective domain with a chain length of 32 amino acids. apoHmp₁₋₅₅ contains all the apoHmp₁₋₃₂ amino acids, plus the next native 23 amino acids in the apoHmp sequence. apoHmp₁₋₁₄₀ denotes the entire first domain of apoHmp (140 amino acids). apoHmp₁₋₁₈₉ contains the entire first domain of apoHmp outside of the ribosomal exit tunnel. PIR was used to elucidate any differences in stability between foldable proteins and IDPs (91 amino acids).

Figure S5. a) Puromycin mimics the 3' end of the amino acyl tRNA and covalently attaches to nascent chains, promoting their release from peptidyl tRNA. This process is accompanied by a significant decrease in molecular weight. b) Low-pH SDS-PAGE is employed to quantify peptidyl-tRNA (PT) band intensities as a function of urea concentration. Puromycin is unable to perform its function at high urea concentration because of pervasive PTC unfolding (SI Appendix, Fig. S1). c) Representative low-pH gels showing that peptidyl tRNA bands are

unaffected by high urea concentrations. Addition of puromycin (1 mM) results in a decrease in peptidyl-tRNA (PT) band intensities, at low urea concentration. **d)** Block diagram mapping apparent unfolding free energy values (ΔG° app,unfold). Error bars denote standard errors based on 2-7 experiments. **e)** Representative urea titration curves corresponding to the raw data in panel c. Data were fit to a two-state unfolding expression (see Methods section for details). **f)** P-value table for a two-tailed Student's test assuming unequal variances (Welch's t-test). Green and orange boxes denote statistically different and statistically equivalent data, respectively, according to a \geq 95% confidence interval.

Figure S6. a) The r-proteins of the *E. coli* 70S ribosome include 32 tryptophans (Trp, magenta). 16 and 16 Trps are located within the 50S and 30S subunits, respectively (PDB IDs: 2WWL and 2WWQ). b) Scheme illustrating the methodology followed to assess r-protein stability. c) Trp fluorescence-emission bands become red-shifted at increasing urea concentrations due to changes towards a more polar medium. d) Representative urea titration curves from steady-state fluorescence of RNCs of snc-tRNA, apoHmp1-32, apoHmp108-140, apoHmp152-184, apoHmp230-262, apoHmp263-295, apoHmp371-403, apoHmp1-55, apoHmp1-140, apoHmp1-189 and PIR respectively. The symbol funf denotes change in the fraction of unfolded r-proteins (eq. 4). e) Apparent unfolding free energies (ΔG°app,unfold). Uncertainties are reported as ± SE for n=2-3. f) P-value table for the two-tailed Student's T-test (Welch's test) comparing ΔG°app,unfold values. Green and orange boxes denote statistically different and statistically equivalent data, respectively, according to a 95% confidence interval.

Figure S7. Time-course experiments for apoHmp₁₋₅₅ are shown at 0.45 M urea. There is no change in spectral shift as incubation time is dramatically increased.

Figure S8. Identification of ribosomal proteins crosslinked to apoHmp₁₋₁₄₀ RNCs via Western blotting. Left, low-pH 10% SDS-PAGE analysis of N-terminal fluorescently-labeled apoHmp₁₋₁₈₉ RNCs generated via transcription-translation in an *E. coli Dtig* S30 cell-free system followed by Western blotting (right) employing antibodies against ribosomal proteins (a) L24 and (b) L29. See Methods for Western blotting and antibodies details, representative data, out of n = 2, are displayed.

Figure S9. A proposed disassembly model for empty ribosomes and ribosome-bound nascent chains. (a) Briefly, empty ribosomes begin to dissociate from one another at c.a. 1 M urea. At > 2 M urea empty ribosomes experience r-protein and rRNA unfolding. (b) Briefly, RNCs begin to dissociate from one another at c.a. 1-2 M urea. At > 3 M urea empty ribosomes experience r-protein and rRNA unfolding.

Figure S10. (a) Low pH 10% SDS-PAGE gel showing apoHmp₁₋₁₄₀ with no Hsp70 chaperones added (K/J/E) and physiologically relevant concentrations, respectively. (b) ApoHmp₁₋₁₄₀ at various concentrations of trigger factor molecular chaperone. Concentration of trigger factor increases from left gel to right gel. See methods for more information about chaperone concentration.

Figure S11. Identification of ribosomal proteins crosslinked to apoHmp₁₋₁₈₉ RNCs via Western blotting. Left, low-pH 10% SDS-PAGE analysis of N-terminal fluorescently-labeled apoHmp₁₋₁₈₉ RNCs generated via transcription-translation in an *E. coli Dtig* S30 cell-free system followed by Western blotting (right) employing antibodies against ribosomal proteins L24 and L29. See Methods for Western blotting and antibodies details, representative data, out of n = 2, are displayed.

SUPPORTING TABLES

Supporting Table S1

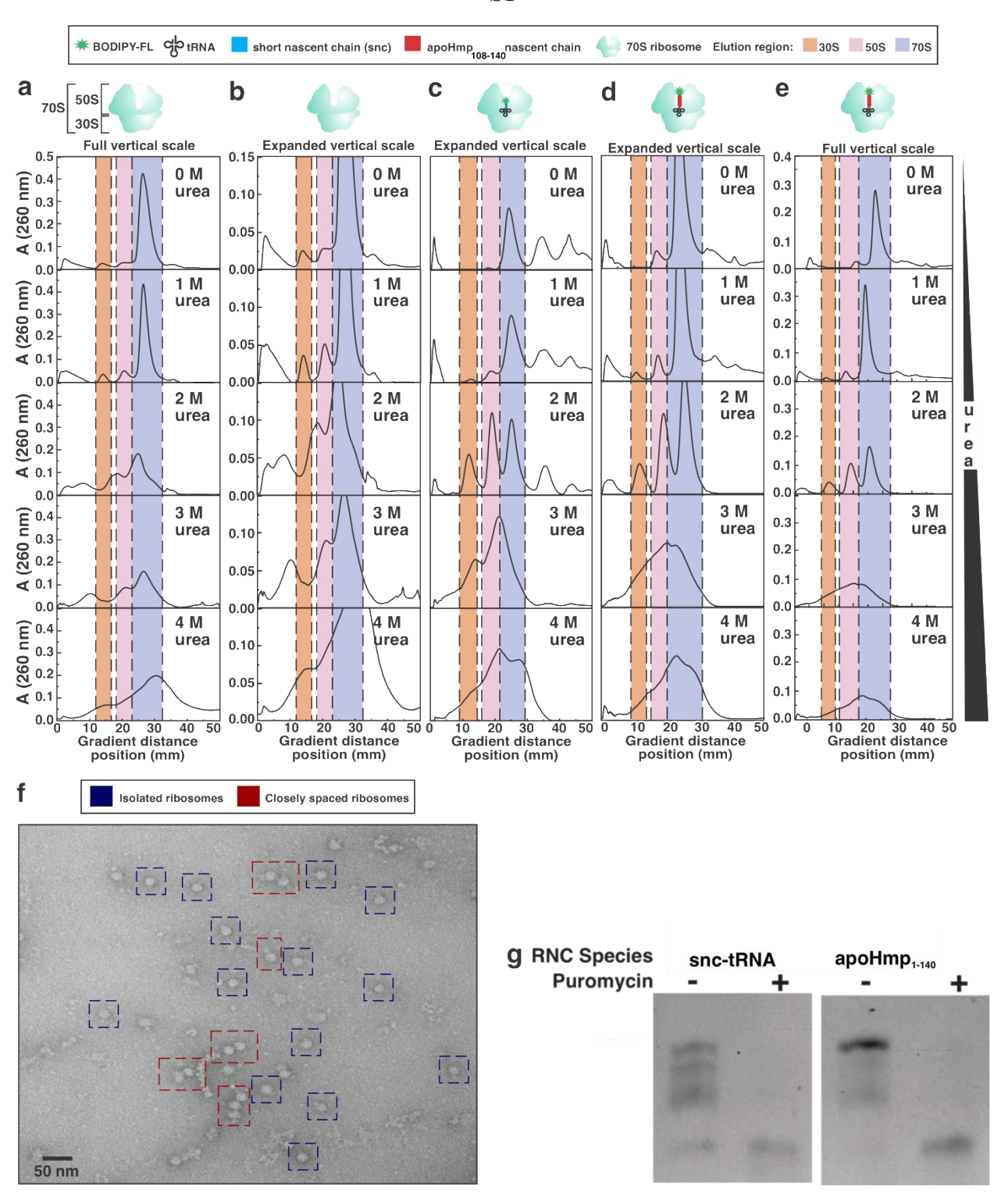
RNC	Technique	Interacting ribosomal protein	Reference
	Proteins with an N-termin	al signal sequence	
Leader peptidase	photo-crosslinking	L4, L22 and L23	(37)
Two regulatory ribosome stalling peptides	cryo-EM	L4 and L17	(35)
Transmembrane segment of 111p membrane protein	photo-crosslinking	not determined	(39)
Signal anchor of FtsQprotein	photo-crosslinking	L23 and L29	(40)
pOmt	photo-crosslinking	L23 and L24	(41)
EsP1-25	photo-crosslinking	L23 and L24	(42)
Prote	photo-crosslinking	Some-stalling sequence L22 and L24	(43)
TnaC	cryo-EM	L22	(44)
SecM	cryo-EM	L22 and L23	(45)
SecM	mutagenesis	L22	(46)
SecM	cryo-EM	L23	(33)
Signal anchor of	photo-crosslinking	RpI4, Rp17 and RpI29	(47)
Dap2 Protein SecM	NMR	not determined	(48)
	Proteins with no N- or	C-terminal tag	
Phosphorylated insulin receptor (PIR)	chemical crosslinking	L23	(1)

Supporting Table S2

Construct	Oligo-nucleotide sequence	ΔG°unf
Anti-ssrA	TTAAGCTGCTAAAGCGTAGTTTTCGTCGTTTTGCGACTA	54.2
snc-tRNA	GCGTCAAGCAT	12.4
ApoHmp ₁₋₃₂	CATACGGTCGTAGAAATGGGCGGTTAACTTTGGCCCCG	57.9
ApoHmp108-140	TTAGTTATAGATTTCCGCCTCGCGATTGATAAATACAT	48.9
ApoHmp ₁₅₂₋₁₈₄	TATTCTGCCACTGCGCCACCGTCGACCGGC	49.2
ApoHmp230-262	CGGAGCGACCAGTTTCACGACATCGCCACCA	49.0
ApoHmp263-295	ATGGAACCAGTTCACTTGTGCTGTGTGGCCTGCTTTTG	54.9
ApoHmp ₃₇₁₋₄₀₃	CAGCACCTTATGCGGGCCAAAGCATTCGTAATG	47.9
ApoHmp ₁₋₅₅	AAGTGCAACTAAGCGGTAATGCGGACCAATGAG	49.3
ApoHmp1-140	TTAGTTATAGATTTCCGCCTCGCGATTGATAAATACAT	48.9
ApoHmp1-189	GAGATATTGCCCCGGACGGTATTCTGCCACTGCGCCAC	59.2
PIR ₁₋₉₁	GTGGTGGTGGTGGTGCTCGAGTGCGGCCGCAAGCT	63.9

SUPPORTING FIGURES

S1

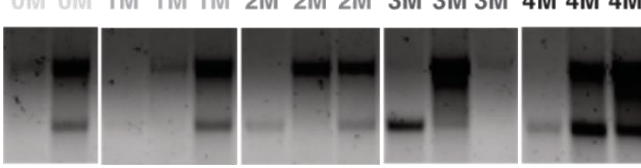


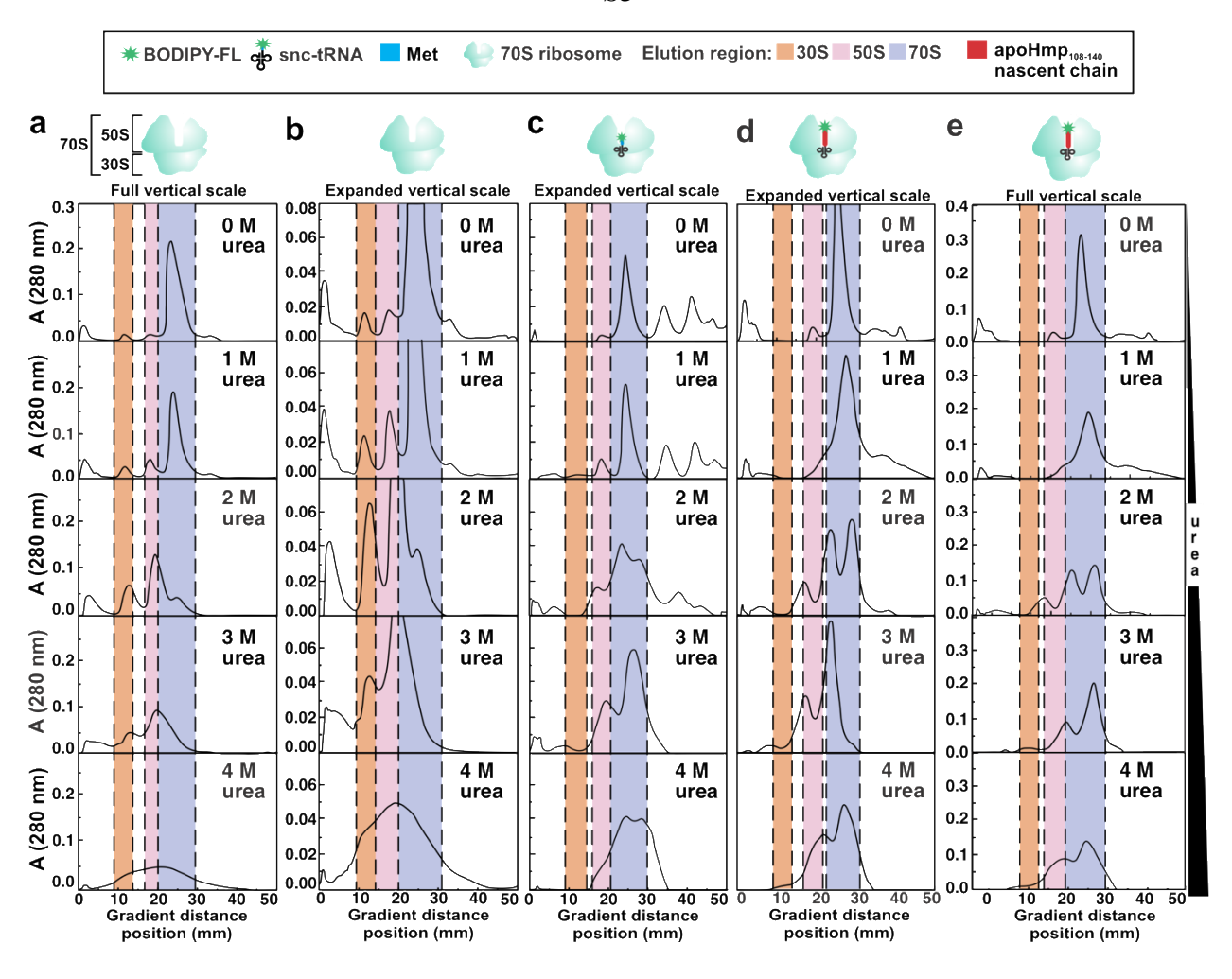


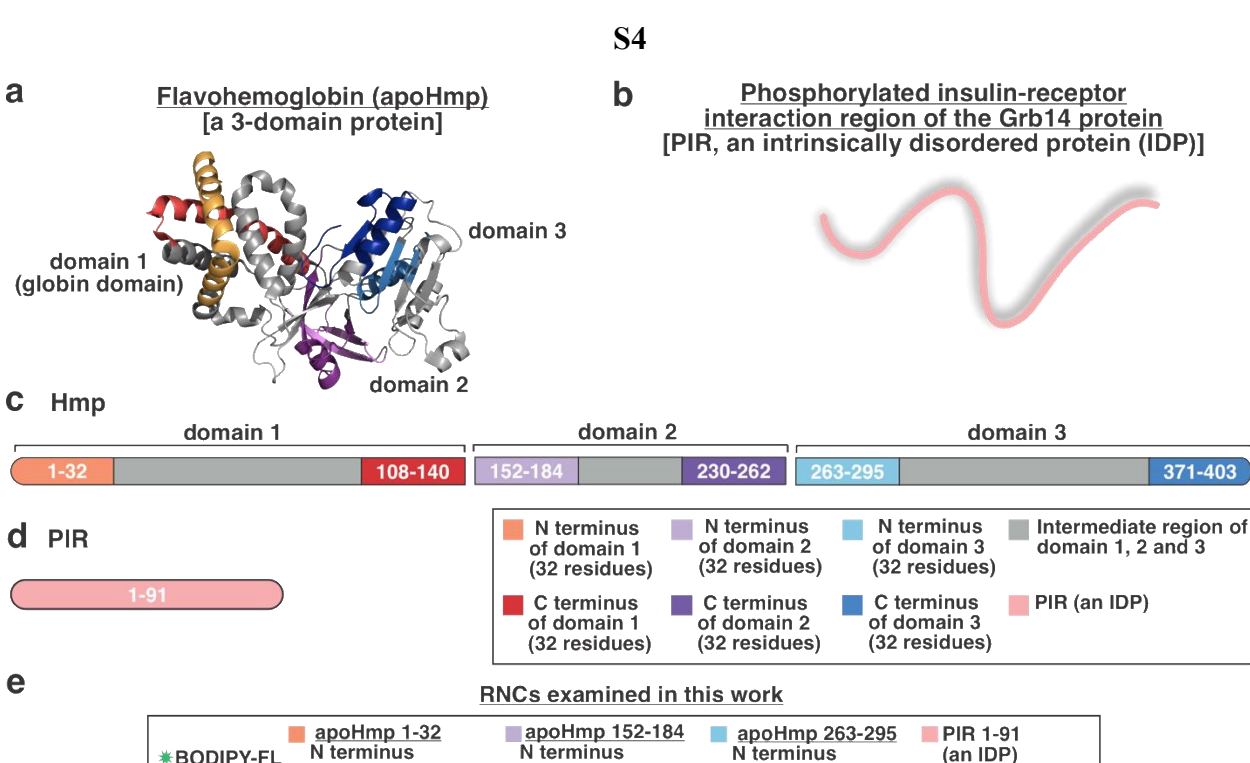
b Ribosomal Subunit 508 708 308 508 708 308 508 708 308 508 708 308 508 708

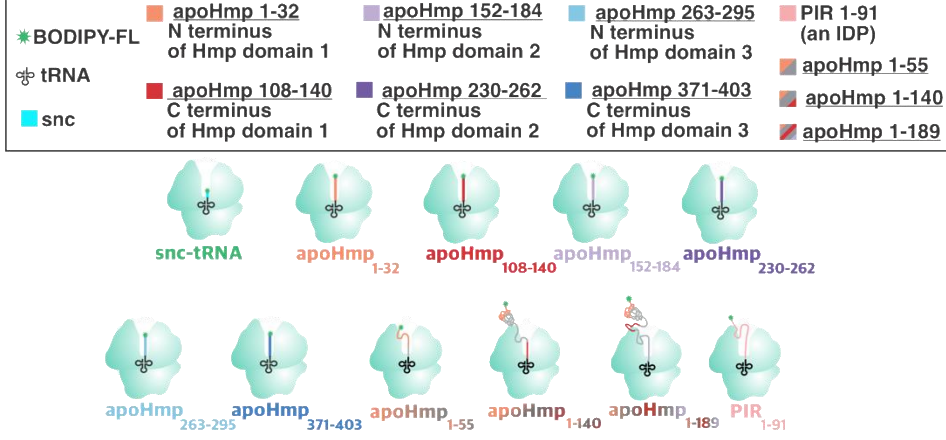
Urea Concentration OM OM 1M 1M 1M 2M 2M 2M 3M 3M 3M 4M 4M 4M

23S rRNA 16S rRNA



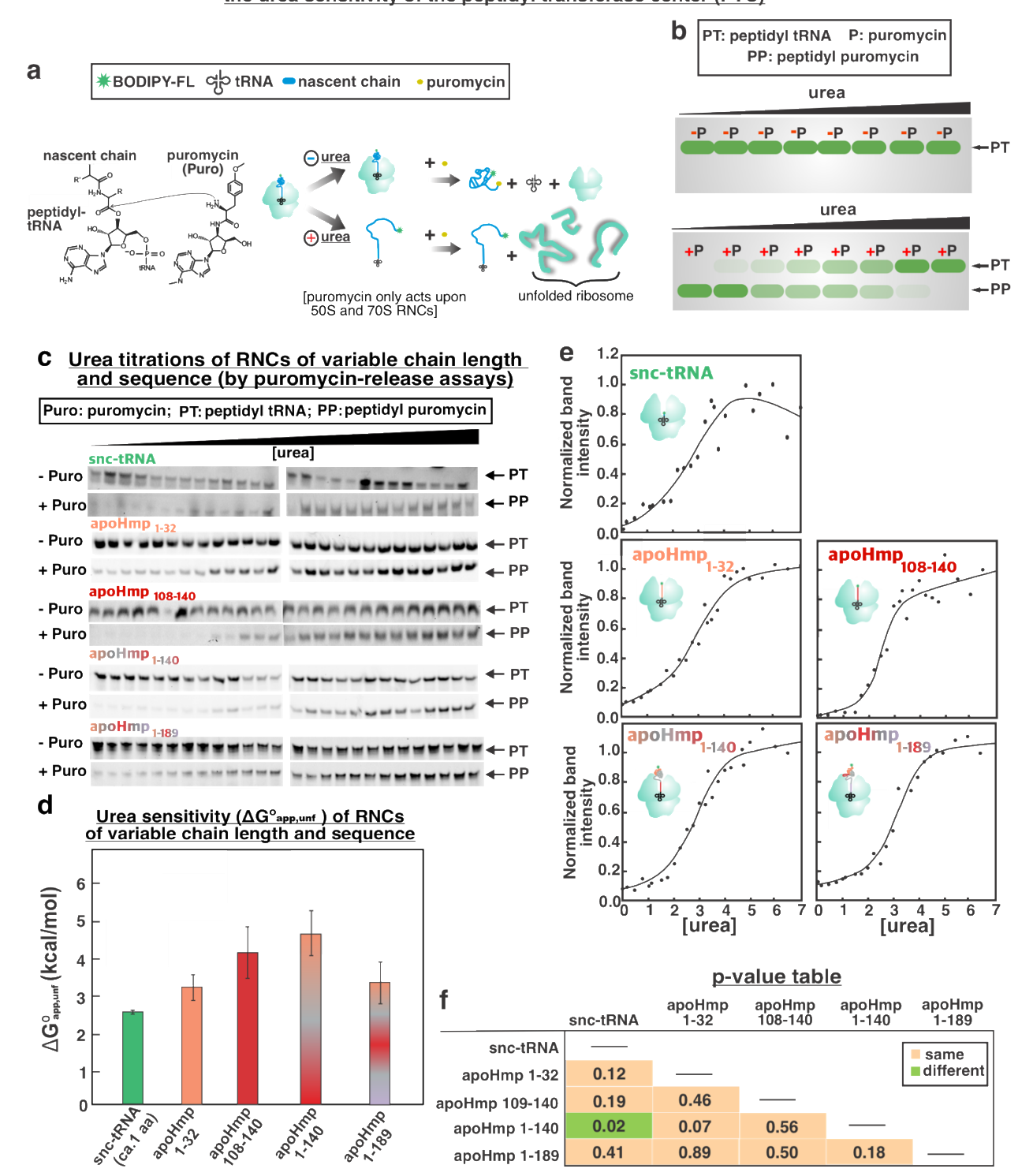


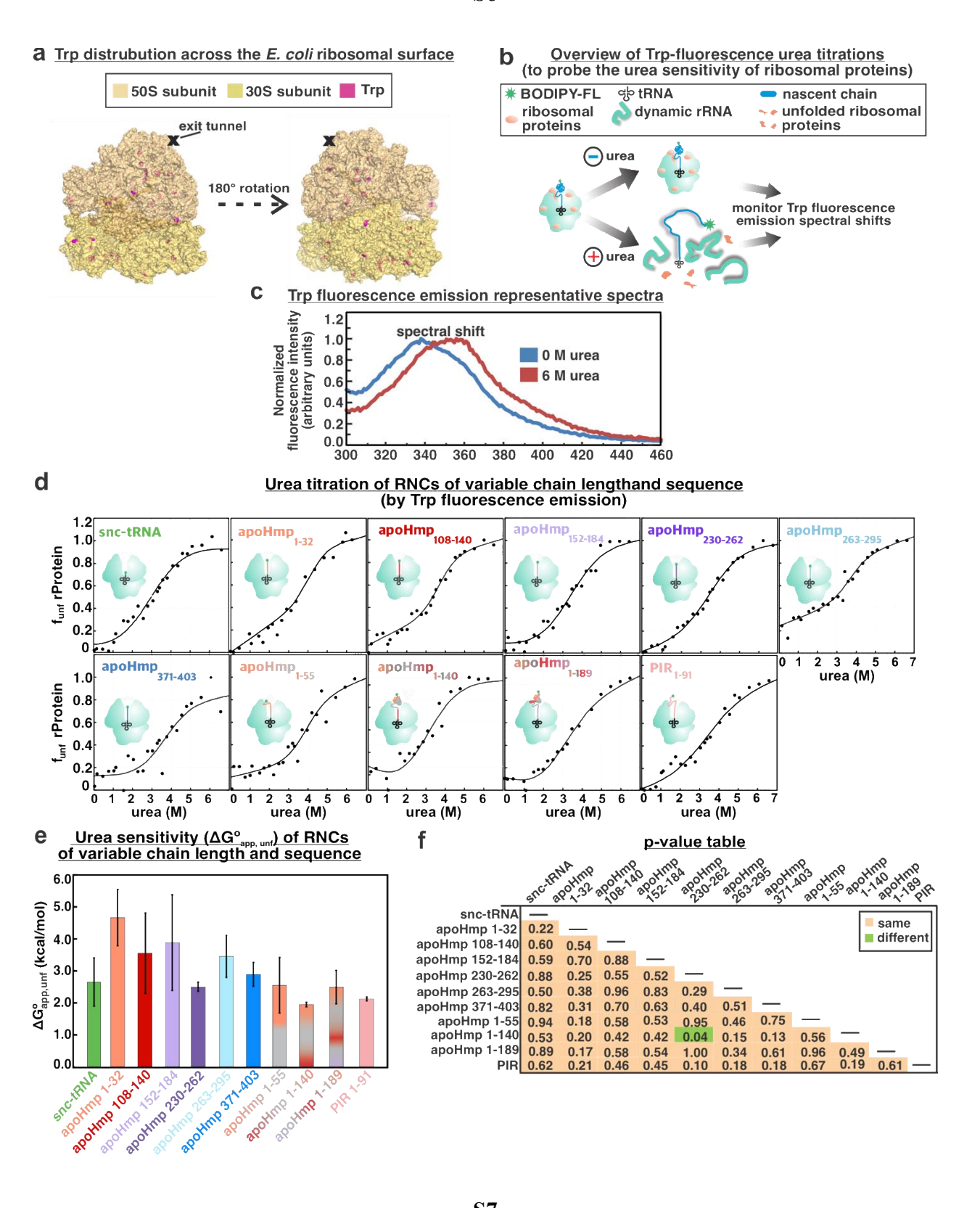


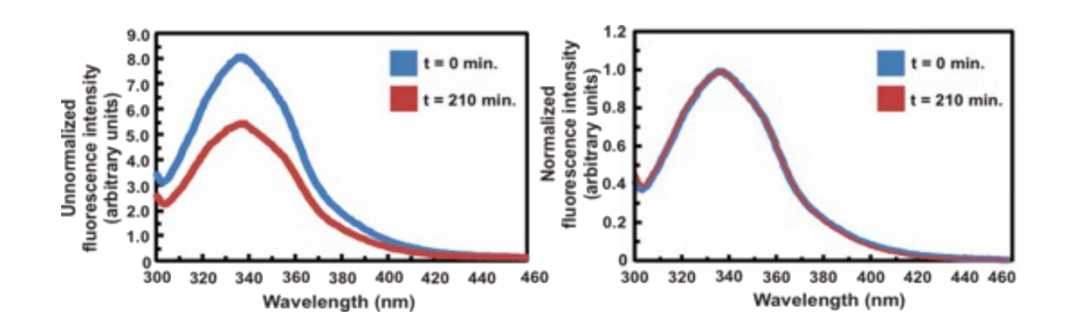


Puromycin/urea titrations: experimental procedure to study the urea sensitivity of the peptidyl transferase center (PTC)

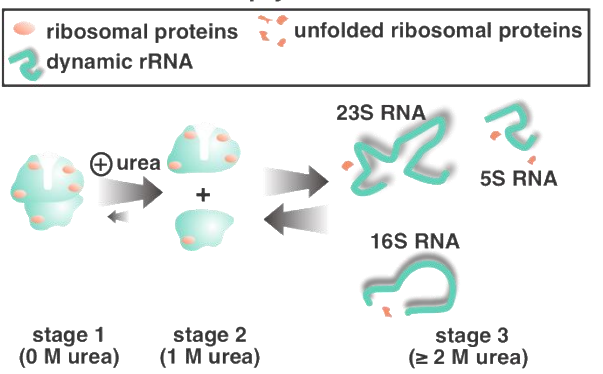
S5







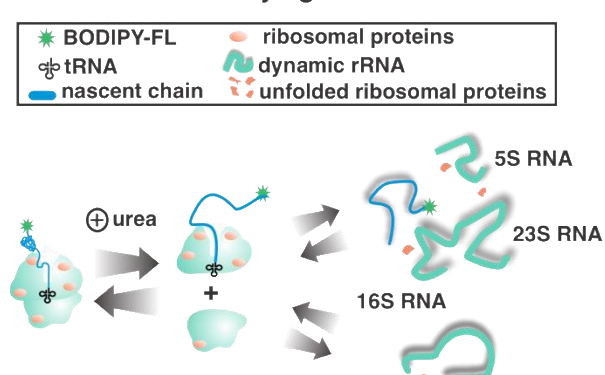
a <u>Proposed disassembly mechanism</u> <u>of empty ribosomes</u>



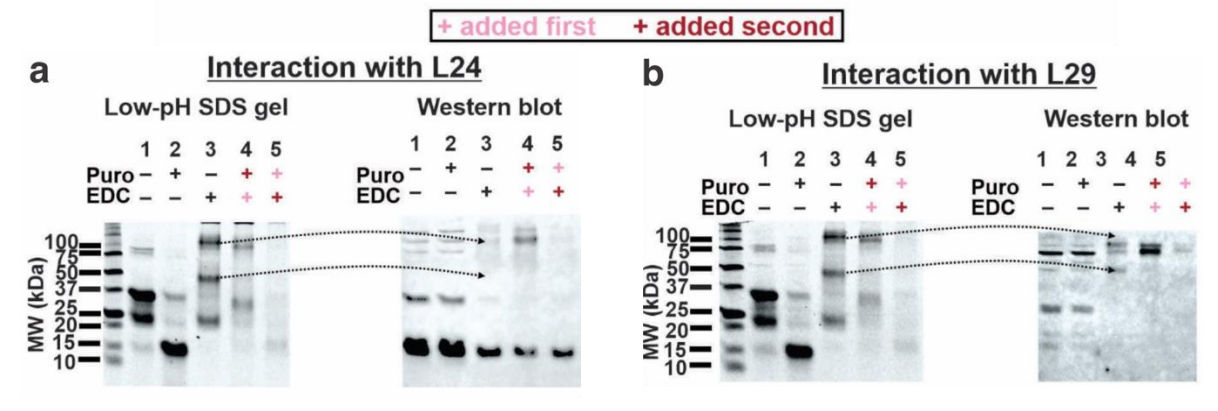
b Proposed disassembly mechanism of ribosomes carrying a nascent chain

stage 2 (1-2 M urea)

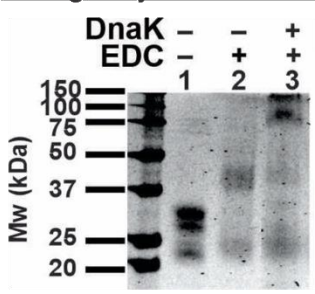
stage 1 (0 M urea)



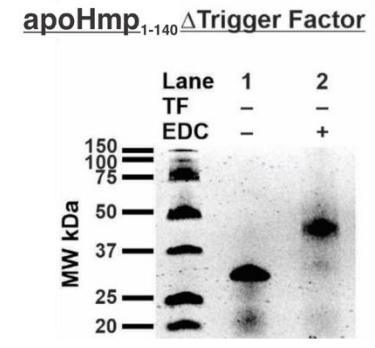
stage 3 (3-4 M urea)

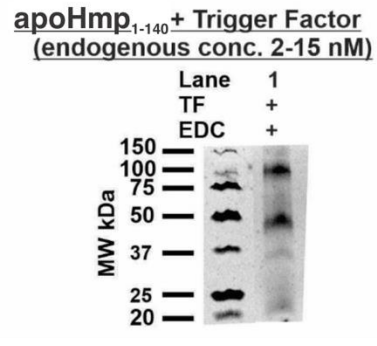


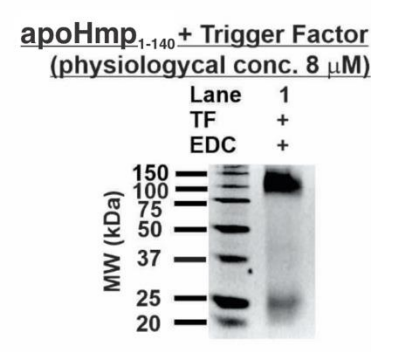
a <u>apoHmp₁₋₁₄₀ interacts with K/J/E at</u> <u>physiologically relevant concentrations</u>



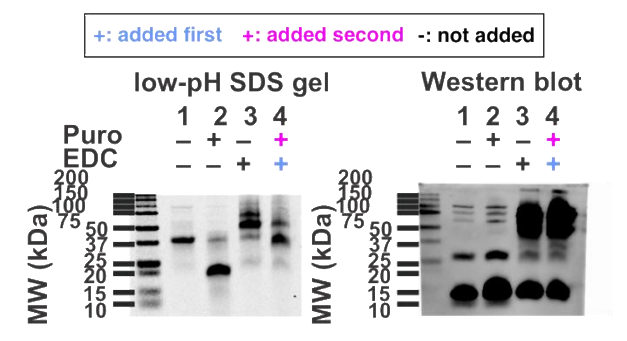
b <u>apoHmp₁₋₁₄₀ RNCs interact with ribosomal proteins and TF chaperone</u> at both endogenous and physiologically relevant concentrations



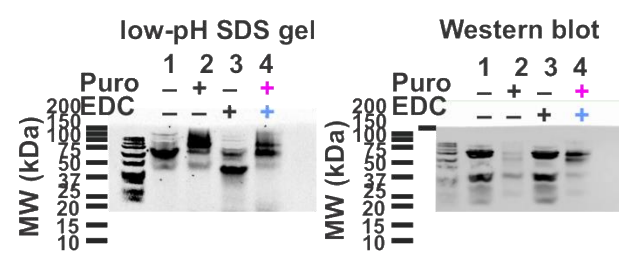




S11
apoHmp,..ss.does not interact with L24
outside of the ribosomal tunnel exit



apoHmp₁₋₁₈₉ does not interact with L29 outside of the ribosomal tunnel exit



SUPPORTING REFERENCES

- 1. V. Guzman-Luna, A. M. Fuchs, A. J. Allen, A. Staikos, S. Cavagnero, An intrinsically disordered nascent protein interacts with specific regions of the ribosomal surface near the exit tunnel. *Communications biology* **4**, 1-17 (2021).
- 2. J. P. Ellis, C. K. Bakke, R. N. Kirchdoerfer, L. M. Jungbauer, S. Cavagnero, Chain dynamics of nascent polypeptides emerging from the ribosome. *Acs Chemical Biology* 3, 555-566 (2008).
- 3. M. Behrmann *et al.*, Requirements for the translocation of elongation-arrested, ribosome-associated OmpA across the plasma membrane of Escherichia coli. *J. Biol. Chem.* **273**, 13898-13904 (1998).
- H. Donis-Keller, Site specific enzymatic cleavage of RNA. Nucleaic Acid Research 7, 179-192 (1979).
- 5. D. N. Wilson, R. Beckmann, The ribosomal tunnel as a functional environment for nascent polypeptide folding and translational stalling. *Curr. Opin. Struct. Biol.* **21**, 274-282 (2011).
- 6. A. Günzl, Z. Palfi, A. Bindereif, Analysis of RNA-protein complexes by oligonucleotide-targeted RNase H digestion. *Methods* **26**, 162-169 (2002).
- 7. R. F. Dos Santos, C. M. Arraiano, J. M. Andrade, "Isolation and Analysis of Bacterial Ribosomes Through Sucrose Gradient Ultracentrifugation" in RNA Chaperones.

 (Springer, 2020), pp. 299-310.
- 8. A. Robinson, J. Sykes, A comparison of the unfolding and dissociation of the large ribosome subunits from Rhodopseudomonas· spheroides NCIB 8253 and Escherichia coli MRE 600. *Biochem. J.* **133**, 739-747 (1973).

- 9. K. Hosokawa, Binding of 5 S ribosomal ribonucleic acid to the unfolded 50 S ribosomes of Escherichia coli II. *J. Biol. Chem.* **245**, 5880-5887 (1970).
- 10. M. Tal, Metal ions and ribosomal conformation. *Biochimica et Biophysica Acta (BBA)-Nucleic Acids and Protein Synthesis* **195**, 76-86 (1969).
- 11. S. Natori, H. Maruta, D. i. Mizuno, Unfolding of Escherichia coli ribosomes by phosphate ion in the presence of oligonucleotides. *J. Mol. Biol.* **38**, 109-119 (1968).
- 12. D. L. Weller, Y. Shechter, D. Musgrave, M. Rougvie, J. Horowitz, Conformational changes in Escherichia coli ribosomes at low magnesium ion concentrations.

 **Biochemistry 7, 3668-3675 (1968).
- 13. R. J. Beller, N. H. Lubsen, Effect of polypeptide chain length on dissociation of ribosomal complexes. *Biochemistry* **11**, 3271-3276 (1972).
- 14. N. Belitsina, A. Spirin, Studies on the structure of ribosomes: IV. Participation of aminoacyl-transfer RNA and peptidyl-transfer RNA in the association of ribosomal subparticles. *J. Mol. Biol.* **52**, 45-55 (1970).
- 15. E. Z. Ron, R. E. Kohler, B. D. Davis, Magnesium ion dependence of free and polysomal ribosomes from Escherichia coli. *Journal of molecular biology* **36**, 83-89 (1968).
- 16. M. E. Roberts, I. Walker, Structural studies on Escherichia coli ribosomes: III.
 Denaturation and sedimentation of ribosomal subunits unfolded in urea. *Biochimica et Biophysica Acta (BBA)-Nucleic Acids and Protein Synthesis* 199, 184-193 (1970).
- 17. A. J. Samelson, M. K. Jensen, R. A. Soto, J. H. D. Cate, S. Marqusee, Quantitative determination of ribosome nascent chain stability. *Proceedings of the National Academy of Sciences of the United States of America* **113**, 13402-13407 (2016).

- 18. P. Spitnik-Elson, B. Greenman, The detachment of ribosomal proteins by urea: evidence for non-electrostatic RNA-protein interaction in the ribosome. *FEBS Lett.* **17**, 187-192 (1971).
- 19. H.-C. Hung, G.-G. Chang, Multiple Unfolding Intermediates of Human Placental Alkaline Phosphatase in Equilibrium Urea Denaturation. *Biophys. J.* **81**, 3456-3471 (2001).
- 20. J. Shine, L. Dalgarno, The 3'-terminal sequence of Escherichia coli 16S ribosomal RNA: complementarity to nonsense triplets and ribosome binding sites. *Proceedings of the National Academy of Sciences* **71**, 1342-1346 (1974).
- 21. F. Mohammad, R. Green, A. R. Buskirk, A systematically-revised ribosome profiling method for bacteria reveals pauses at single-codon resolution. *Elife* **8**, e42591 (2019).
- G. Yusupova, L. Jenner, B. Rees, D. Moras, M. Yusupov, Structural basis for messenger
 RNA movement on the ribosome. *Nature* 444, 391-394 (2006).
- 23. F. Brandt *et al.*, The Native 3D Organization of Bacterial Polysomes. *Cell* **136**, 261-271 (2009).
- 24. R. M. Oliver, "Negative stain electron microscopy of protein macromolecules" in Methods in enzymology. (Elsevier, 1973), vol. 27, pp. 617-672.
- 25. M. B. Yarmolinsky, L. Gabriel, Inhibition by puromycin of amino acid incorporation into protein. *Proceedings of the National Academy of Sciences* **45**, 1721-1729 (1959).
- I. Wohlgemuth, M. Beringer, M. V. Rodnina, Rapid peptide bond formation on isolated
 50S ribosomal subunits. *EMBO reports* 7, 699-703 (2006).

- 27. R. N. Kirchdoerfer, J. J. T. Huang, M. K. Isola, S. Cavagnero, Fluorescence-based analysis of aminoacyl- and peptidyl-tRNA by low-pH sodium dodecyl sulfate-polyacrylamide gel electrophoresis. *Anal. Biochem.* **364**, 92-94 (2007).
- 28. M. M. Santoro, D. W. Bolen, Unfolding free-energy changes determined by the linear extrapolation method.1.unfolding of phenylmethanesulfonyl alpha-chymotrypsin using different denaturants. *Biochemistry* **27**, 8063-8068 (1988).
- 29. C. N. Pace, Measuring and increasing protein stability. *Trends Biotechnol.* **8**, 93-98 (1990).
- A. Bonincontro *et al.*, Differential stability of E. coli ribosomal particles and free RNA towards thermal degradation studied by microcalorimetry. *Biophys. Chem.* 75, 97-103 (1998).
- 31. J. R. Warren, J. A. Gordon, On the refractive indices of aqueous solutions of urea. *The Journal of Physical Chemistry* **70**, 297-300 (1966).
- 32. C. A. Schneider, W. S. Rasband, K. W. Eliceiri, NIH Image to ImageJ: 25 years of image analysis. *Nat. Methods* **9**, 671-675 (2012).
- 33. S. Wang *et al.*, The molecular mechanism of cotranslational membrane protein recognition and targeting by SecA. *Nat. Struct. Mol. Biol.* **26**, 919-929 (2019).
- 34. L. Lindahl *et al.*, Organization of ribosomal-protein genes in escherichia-coli. 7. mapping of ribosomal-protein genes by invitro protein-synthesis using dna fragments of lambda-fus3 transducing phage dna as templates. *J. Biol. Chem.* **252**, 7365-7383 (1977).
- J. M. Beechem, L. Brand, Time-resolved fluorescence of proteins. *Annu. Rev. Biochem.*54, 43-71 (1985).

- A. P. Demchenko, *Ultraviolet spectroscopy of proteins* (Springer Science & Business Media, 2013).
- 37. G. Weber, Fluorescence-polarization spectrum and electronic-energy transfer in tyrosine, tryptophan and related compounds. *Biochem. J.* **75**, 335 (1960).
- 38. F. Teale, G. Weber, Ultraviolet fluorescence of the aromatic amino acids. *Biochem. J.* **65**, 476 (1957).
- 39. C. A. Woolhead, P. J. McCormick, A. E. Johnson, Nascent membrane and secretory proteins differ in FRET-detected folding far inside the dribosome and in their exposure to ribosomal proteins. *Cell* **116**, 725-736 (2004).
- 40. R. S. Ullers *et al.*, Interplay of signal recognition particle and trigger factor at L23 near the nascent chain exit site on the Escherichia coli ribosome. *The Journal of cell biology* **161**, 679-684 (2003).
- 41. G. Eisner, M. Moser, U. Schäfer, K. Beck, M. Müller, Alternate Recruitment of Signal Recognition Particle and Trigger Factor to the Signal Sequence of a Growing Nascent Polypeptide. *J. Biol. Chem.* **281**, 7172-7179 (2006).
- 42. J. H. Peterson, C. A. Woolhead, H. D. Bernstein, The conformation of a nascent polypeptide inside the ribosome tunnel affects protein targeting and protein folding. *Mol. Microbiol.* 78, 203-217 (2010).
- 43. L. R. Cruz-Vera, S. Rajagopal, C. Squires, C. Yanofsky, Features of Ribosome-PeptidyltRNA Interactions Essential for Tryptophan Induction of tna Operon Expression. *Mol. Cell* **19**, 333-343 (2005).
- 44. B. Seidelt *et al.*, Structural Insight into Nascent Polypeptide Chain–Mediated Translational Stalling. *Science* **326**, 1412-1415 (2009).

- 45. S. Bhushan *et al.*, Structural basis for translational stalling by human cytomegalovirus and fungal arginine attenuator peptide. *Mol. Cell* **40**, 138-146 (2010).
- 46. H. Nakatogawa, K. Ito, The ribosomal exit tunnel functions as a discriminating gate. *Cell* 108, 629-636 (2002).
- 47. Y. Zhang, T. Wolfle, S. Rospert, Interaction of nascent chains with the ribosomal tunnel proteins Rpl4, Rpl17, and Rpl39 of Saccharomyces cerevisiae. *J. Biol. Chem.* **288**, 33697-33707 (2013).
- 48. C. Burridge *et al.*, Nascent chain dynamics and ribosome interactions within folded ribosome-nascent chain complexes observed by NMR spectroscopy. *Chemical Science* **12**, 13120-13126 (2021).